Childs Nerv Syst (2011) 27:523–564
DOI 10.1007/s00381-010-1358-9

REVIEW PAPER

Embryology and bony malformations of the craniovertebral junction

Dachling Pang · Dominic N. P. Thompson

Received: 21 November 2010 / Accepted: 23 November 2010 / Published online: 31 December 2010

Abstract
Background The embryology of the bony craniovertebral junction (CVJ) is reviewed with the purpose of explaining the genesis and unusual configurations of the numerous congenital malformations in this region. Functionally, the bony CVJ can be divided into a central pillar consisting of the basiocciput and dental pivot and a two-tiered ring revolving round the central pivot, comprising the foramen magnum rim and occipital condyles above and the atlantal ring below. Embryologically, the central pillar and the surrounding rings descend from different primordia, and accordingly, developmental anomalies at the CVJ can also be segregated into those affecting the central pillar and those affecting the surrounding rings, respectively.
Discussion A logical classification of this seemingly unwieldy group of malformations is thus possible based on their ontogenetic lineage, morbid anatomy, and clinical relevance. Representative examples of the main constituents of this classification scheme are given, and their surgical treatments are selectively discussed.

Keywords Craniovertebral junction · Congenital malformations · Genetic control · Occipital–cervical instability · Cord compression · Occipital–cervical fusion · Primary somitogenesis · Sclerotomal resegmentation · Embryology · Malformation · Surgery

D. Pang
Department of Neurological Surgery,
University of California, Davis,
Sacramento, CA, USA

D. Pang
Regional Centre of Pediatric Neurosurgery,
Kaiser Foundation Hospitals of Northern California,
Oakland, CA, USA

D. N. P. Thompson
Department of Paediatric Neurosurgery,
Great Ormond Street Hospital for Children NHS Trust,
Great Ormond Street,
London, UK

D. Pang (✉)
Department of Paediatric Neurosurgery,
Kaiser Permanente Medical Center,
280 W. MacArthur Blvd,
Oakland, CA 94611, USA
e-mail: PangTV@aol.com

Introduction

The bony craniovertebral junction (CVJ) can be conceptually divided into two components with respect to the governance of intersegmental movements and functional space for the nervous system. The first component consists mainly of a central pivot made up of the dens and the C_2 vertebral body, but the basiocciput, though anatomically part of the foramen magnum, is embryologically and functionally in vertical linearity with the dens and is thus part of the central pillar. The second component consists of two ringed structures surrounding the central pivot, albeit eccentrically. They are the foramen magnum ring, comprising the lateral portion of the basiocciput (clivus), the exoccipital including the occipital condyles, and the opisthion; and the atlantal ring, with its anterior and posterior arches and lateral masses. These two superimposing rings transmit the lower brainstem and upper cervical spinal cord, whilst permitting limited rotatory and flexion–extension motions upon each other and round the dental pivot. Straddling these two rings and anchoring upon them are the stabilizing ligaments between the pivot and the rings: the alar and apical dental ligaments at the up-side of the

pivot, the transverse atlantal ligament (TAL) across the main dental shaft, and the arching mantle of the tectorial membrane and cruciate ligament, strapping the clivus to the whole of the dens–axis assembly.

Not surprisingly, the anatomical division of the CVJ into axial and flanking components has close analogy in the embryology of this region. The constituents of the central pillar are all derived from the axial portion of the occipital and upper two cervical sclerotomes, whereas the ring structures all come from the lateral portion of these same sclerotomes as well as from a small sclerotomal off-shoot ventral to the notochord called the hypochordal bow (see below). Accordingly, disturbance in the axial sclerotomes produces anomalies of the dens pivot and the basiocciput: the former comprises the various forms of odontoid dysgenesis and the latter the less familiar types of clival abnormalities. A testament to the proximate origins of the dental and clival primordia is readily proclaimed by the large archive of associative syndromes of platybasia, brachybasia, basilar kyphosis, basilar impression, retroflexed dens, and cerebellar ectopia. In contrast, disturbance in the lateral portion of the occipital and upper cervical sclerotomes and hypochordal bow results in anomalies of the "rings", including dysplasia of the lateral clival rim, occipital condyles, the anterior and posterior atlantal arches, and the lateral masses of C_1 and C_2. Table 1 segregates these anomalies by ontogenetic lineages and shows that this seemingly confusing and unwieldy group of malformations are in fact steep in embryological logic.

In keeping with the anatomical division of the CVJ, clinically significant developmental anomalies affecting, respectively, the "pivot" and "rings" also happen to follow more or less a thematic division of instability versus neural compression. Anomalies of the central pivot usually lead to instability, although basilar impression and a retroflexed dens can cause neural impingement. Anomalies of the surrounding rings result in deformity and crowding, but hypoplasia and aplasia of component parts can result in a weakened frame and loss of ligamentous anchorage.

This paper deals first with the normal development and genetic control of the bony CVJ, followed by descriptions of congenital malformations of this region with emphasis on their embryogenesis and clinical relevance. Special considerations of the techniques and pitfalls of fusion and decompression of the occiput–C_1–C_2 complex in young children are provided when applicable.

Embryology of the craniovertebral junction

The presomitic stage

At gastrulation, epiblastic cells from the embryonic plate caudal to the head process invaginate through the primitive streak to form mesoderm on each side of the neural plate,

Table 1 Classification of bony malformations of the CVJ according to embryogenesis

Clinically significant CVJ bony malformations			
Malformations of central pillar		Malformations of surrounding rings	
Disturbance of axial component of occipital sclerotome, proatlas and C_1 resegmented sclerotome		Disturbance of lateral component and hypochordal bows of proatlas and C_1 resegmented sclerotome	
Odontoid dysgeneses	Basioccipital dysgeneses	Proatlas anomalies	C_1 sclerotome anomalies
▪ Aplasia/hypoplasia of odontoid components	▪ Failed midline integration of basioccipital primordium	▪ Hyperplasia of hypochordal bow of proatlas	▪ Aplasia of hypochordal bow of C_1
▪ Disturbance of odontoid synchondroses (IBZ)	– Bifid clivus	– Third occipital condyle	– Aplasia and hypoplasia of anterior C_1 arch
– Os odontoideum	▪ Basioccipital dysplasia	– Pre-basioccipital arch	▪ Aplasia/hypoplasia of lateral sclerotome
– Ossiculum terminale persistens	– Basilar impression	▪ Hyperplasia of exoccipital sclerotome	– Posterior C_1 arch agenesis
▪ Abnormal resegmentation of proatlas centrum	– Platybasia	– Hypertrophic occipital condyle	▪ Combined hypochordal bow and lateral sclerotome dysplasia
– Os avis	– Retroflexed dens	▪ Non-resegmentation of proatlas (anterior homeotic transformation)	– Aplasia of lateral mass and anterior C_1 arch
▪ Failed midline integration of basal dental segment	– Basilar invagination	– Atlas assimilation	– Combined anterior and posterior C_1 arch defects
– Bifid dens	– Basilar kyphosis	▪ Posterior homeotic transformation	– Bifid anterior and posterior C_1 arch

whilst cells from both sides of the dorsal lip of Hensen's node migrate through the primitive pit to integrate into the midline notochord. The embryonic plate thus elongates by new additions to its rear (caudal) aspect [24].

The anterior–posterior (rostrocaudal) polarity of the embryo is determined very early during gastrulation. The prechordal mesoderm rostral to the otic vesicle (and notochord) forms most of the bones and muscles of the head and face without ever developing somites. Caudal to this tissue is the somitic region which extends along the body axis down to the tip of the tail (Fig. 1). The anterior somitic region from the otic vesicle to the blastopore (future anus) corresponds to the future body axis from the occiput to the anus. Here, the epiblastic cells condense to form the parachordal mesoderm on each side of the notochord following systematic ingression movements through the primitive streak. This initially homogenous column of cells, also called presomitic mesoderm (PSM) or segmental plate, subsequently segregates into segmental clusters called somites, which will eventually give rise to the smooth muscle of the dermis, the axial musculature, the vertebral column, and support structures of the peripheral nervous system. After blastopore closure and complete regression of the primitive streak, the gastrulating region for the tail is restricted to a small cluster of cells called the tail bud, located at the caudal tip of the primitive streak. The tail bud functions as a blastema of undifferentiated cells [20, 21].

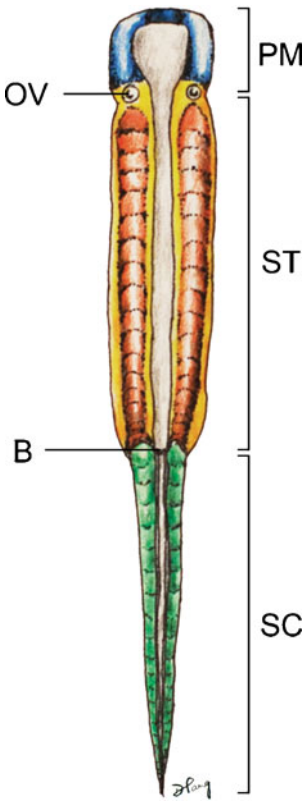

Fig. 1 Vertebrate embryonic plate around gastrulation showing the three main regions of the body plan: The prechordal mesoderm (*PM*) is anterior to the otic vesicle (*OV*). Posterior to the OV to the blastopore (*B*) is the somitic region of the trunk (*ST*), caudal to which is the caudal (tail) somitic region (*SC*)

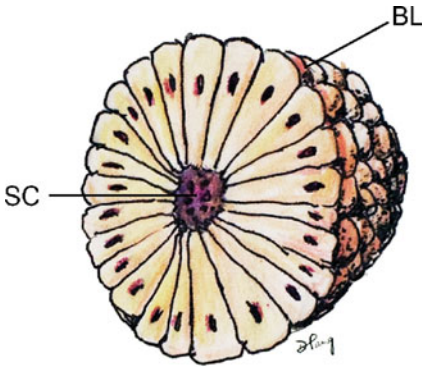

Fig. 2 Somite with radially arranged and polarized epithelial cells surrounding a central cavity, the somitocoele (*SC*) and enveloped by a basal lamina (*BL*)

The presomitic mesoderm and later somites of the caudal and tail regions are therefore not formed by epiblastic ingression but by progenitor condensation in situ.

Primary segmentation: somitogenesis

Prior to the appearance of somites, the PSM remains a loose mesenchyme without specific cellular polarity or stratification pattern alongside the lengthening notochord and neural plate [73]. During somitogenesis, the loose mesenchymal cells of the PSM undergo transformation into tightly apposed epithelial cells with definite polarity and orientation. A newly formed somite is a compact epithelial sphere ("somitomere") composed of a single layer of radially arranged cells with apices pointing towards a central lumen (somitocoele), which contains a few mesenchymal cells [44] (Fig. 2). The epithelial cells have polarized Golgi zones, basally aligned nuclei, and actin molecules near the luminal border, the entire sphere being enveloped by a collagen-containing basal lamina [4]. This epithelial conversion of the PSM is aided by an increase in cell-cell adhesion mediated by a sharp but transient rise in the levels of the calcium-dependent adhesion molecule N-cadherin, of fibronectin, and possibly cytotactin [86].

Somitogenesis begins soon after internalization of the prochordal (head) mesoderm and continues through subsequent production of the body axis. The first somite forms immediately caudal to the otic vesicle [37], followed by sequential transformation such that a new pair of somites is regularly added in a rostrocaudal direction until a fixed species-specific number of somites is reached (Fig. 3). Thus, depending on the stage of gastrulation, the growing column of body mesoderm consists of a rostral section of mature somites already undergoing differentiation into sclerotomes and dermomyotomes, a middle section of new pre-differentiated epithelial somites, and a caudal section of presomitic mesoderm just rostral to the remaining primitive

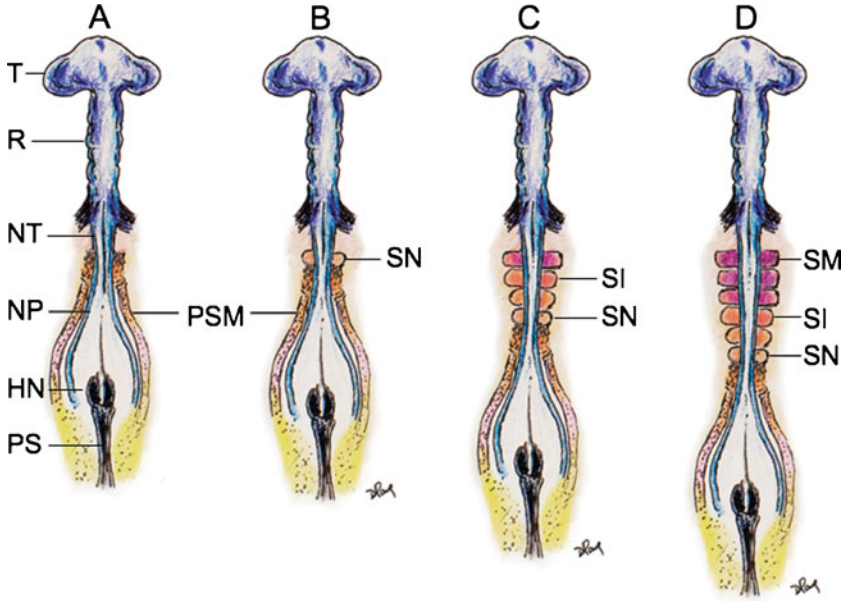

Fig. 3 Primary somitogenesis in a chick embryo. *A* At very early gastrulation, the mostly unneurulated neural plate caudal to the prochordal plate (head process) is flanked on each side by the presomitic (presegmented) mesoderm, or PSM. *B* The first pair of somites are formed just caudal to the otic vesicles. The PSM column elongates from addition of new cells from the caudal embryonic pole rostral to Hensen's node. *C* The new somites (*SN*) are formed in a rostrocaudal direction so that the older more matured somites (*SM*) are rostral, i.e. closer to the cephalic end of the embryo. *D* The older matured somites (*SM*) have undergone dorsoventral differentiation (*purple colour*) into sclerotome and dermomyotome. The intermediate-aged somites (*SI*) (*orange colour*) are pre-differentiated units without dorsoventral specification. The PSM is always at the most caudal end closest to Hensen's node. Rostrocaudal sequential somitogenesis parallels progression of primary neurulation. *HN* Hensen's node, *PS* primitive streak, *T* telencephalon, *R* rhombencephalon, *NT* neural tube, *NP* neural plate

streak, the whole enterprise necessarily evolving in parallel with the neurulating neural plates (Fig. 4).

Current thinking regarding the mechanism of metameric transformation of the PSM follows what is called the "clock and wavefront" model, first proposed by Cooke and Zeeman in 1976. In this model, PSM cells oscillate between a permissive and a non-permissive state for somite formation. These oscillations are phase-linked and controlled cell autonomously by a "segmentation clock." Somitic formation is triggered when cells of the rostral PSM, whilst in the permissive phase of the Clock, are hit by a wavefront of maturation (or determination) that slowly moves caudally along the embryonic axis (Fig. 5). Thus, the Clock generates a temporal periodicity that is translated spatially into the periodic boundaries of the somites [73] (Fig. 6).

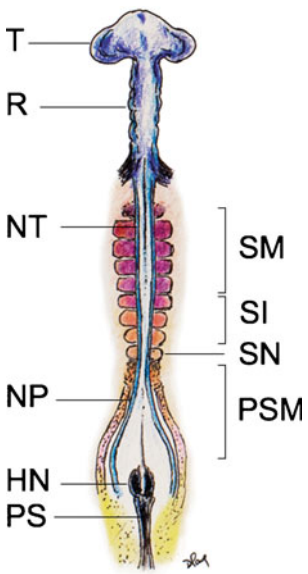

Fig. 4 Chick embryo during sequential somite formation close to the end of gastrulation. The rostral most mesoderm consists of matured somites (*SM*) already having undergone dorsoventral differentiation into dermomyotome and sclerotome, flanking the formed neural tubes (*NT*); followed by the newer intermediate-aged pre-differentiated epithelial somites (*SI*), the new somites (*SN*) and the presomitic mesoderm (*PSM*) on each side of the unneurulated neural plate (*NP*). *HN* Hensen's node, *PS* primitive streak, *T* telencephalon, *R* rhombencephalon

At the molecular level, the phasic oscillation of the segmentation clock is reflected by rhythmic expressions of a class of genes called cycling genes [72]. These genes include the *c-hairy1* family in fish, chick, frog, and mouse, which encode transcription factors such as the split (HES) family and the glycosyl-transferase Lunatic Fringe [27, 54], all tightly involved in the Notch signalling pathway and its ligands, suggesting that periodic Notch activation plays a critical role in the oscillator (Fig. 7). Also, these genes oscillate largely in synchrony in the PSM, suggesting they are downstream of a common cycling activator.

In chick and mouse embryos, the maturation or determination wave is generated by the expression of genes

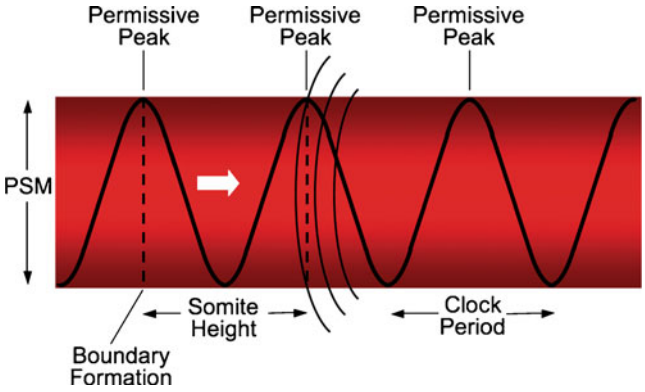

Fig. 5 The clock and wavefront theory of primary somitogenesis. The segmentation clock is a pattern of cell autonomous, phase-linked oscillations of certain "cycling" genes expression within the PSM cells, producing a sinusoidal wave of peaks and troughs of gene products which render the cell either "permissive" or "non-permissive" to changes when "hit" by a moving wavefront. *Block arrow* shows direction of wavefront. When the wavefront (*curved lines*) hits the "permissive" peak of the gene cycle, the cells at that region of the PSM undergo changes which demarcate them from the surrounding uncommitted mesenchyme, causing formation of a boundary zone (*dotted vertical lines*) cutting across the whole width of the PSM column because the clock periods (time lapses between wave peaks) in the PSM are in synchrony. The distance between two boundary lines thus represents the height of a somite, which, in turn, depends on the clock period and, to a certain extent, the velocity of the moving wavefront. Thus, in the clock and wavefront model of primary somitogenesis, time, in terms of the clock period, is transformed into space, in terms of the somite size. The clock periodicity is species specific

which include the fibroblast growth factor gene *fgf8* [80]. It is known that the caudal domain of the PSM is very high in the factor FGF8, which seems to actively maintain the mesenchymal identity of caudal PSM cells. The FGF8 gradient decreases towards the rostral axis, so that at the rostral domain of the PSM where somitogenesis is taking place, FGF8 level is very low. Also, overexpression of *fgf8* in this region results in inhibition of somitogenesis. Thus, the activation of epithelization of PSM cells is negatively regulated by FGF8, whose absence allows the PSM cells to become competent to respond to the clock signal and initiate somitic boundary formation [26]. The limit between the two domains of high (in the caudal PSM) and low (in the rostral PSM) *fgf8* expression therefore marks the determination wavefront of somitogenesis [73] (Fig. 8).

Due to the constant caudal elongation of the body axis during gastrulation and the addition of new PSM cells with strong *fgf8* expression to the rear, the FGF8 gradient is continuously displaced caudally. Accordingly, the determination wavefront also moves slowly in a caudal direction along the body axis. This ensures that the old and new metameric boundaries, at both ends of a new somite, are separated by a distance corresponding to the caudal displacement of the determination wavefront during one period of oscillation of the segmentation clock [72] (Fig. 8). The speed of new somite production is thus linked to the Clock period, which is species-specific: 30 min for zebrafish, 90 min for chick, and 120 min for mouse [68].

Differentiation of the somitic mesenchyme

Within hours after its formation, each somite starts differentiating along its dorsoventral axis. Cells from its ventromedial part lose their epithelial arrangement and migrate towards the notochord to form, with the luminal cells, the mesenchymal sclerotomes [12, 44]. Together with the notochord, the sclerotomes provides exclusive material for the vertebral column. Cells from the dorsolateral part of the somite retain their epithelial arrangement to produce the dermomyotomes (Fig. 9 A, B). The dermomyotomes later subdivides into the dorsal dermatome immediately beneath the ectoderm to give rise to the dermis and its smooth muscles, whilst the disaggregated cells between the dermatome and the sclerotomes remain closely packed as the myotome, forming ultimately the axial skeletal muscles [10, 12, 24] (Fig. 9 C, D).

Whilst specification of the anterior–posterior pattern of the somite appears to be determined very early [1, 38, 45], the dorsoventral values are not intrinsic to the somites. Thus, if the somite were to be surgically rotated dorsoventrally by 180°, sclerotomes still develop in the ventromedial position whilst the dermomyotomes remain dorsolateral. Moreover, a dorsally implanted notochord represses dermatomal differentiation but encourages

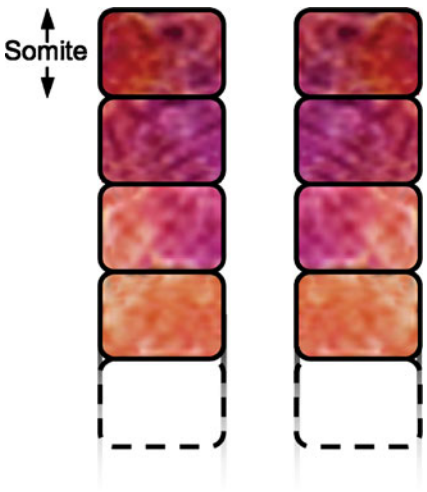

Fig. 6 Periodic boundary formation across the width of the PSM column along its rostrocaudal axis causes segregated somites to form sequentially. The distance between two adjacent boundaries represents the longitudinal dimension of a somite

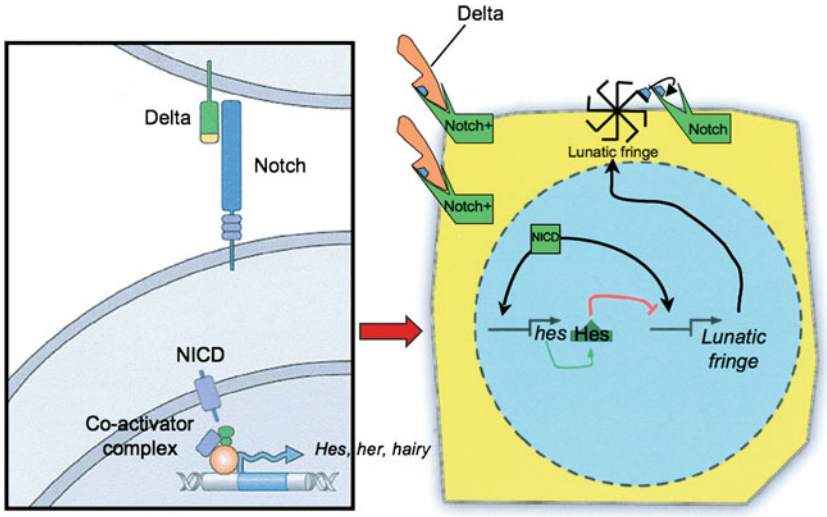

Fig. 7 The molecular basis of the segmentation clock. A ligand (e.g. Delta) is bound to the surface Notch signalling receptor, whose intracellular domain (NICD) then detaches from the cell membrane and enters the nucleus, where it co-activates cycling genes of the *C-hairy 1* family, encoding transcription factors such as HES, HER, HAIRY and Lunatic Fringe. In chick, Lunatic Fringe is known to recycle back to the cell surface, where it "enables" the surface Notch signalling receptor to accept another ligand. The repetitive working of this simplified cycling gene model is the underlying mechanism of the oscillating segmentation clock

sclerotomal formation dorsally, whilst notochord ablation completely prevents sclerotomal appearance [24] (Fig. 10). These findings suggest that the dorsoventral differentiations of the somite depend on appositional instructions from the notochord, very possibly through sonic hedgehog (*Shh*) expression [47] (Fig. 11).

"Resegmentation" of the sclerotome

The term "resegmentation" was originated by Remak in 1855 ("Neugliederung") [79] and remains still a subject of controversies [16, 24]. It refers to the fact that the early metameric boundaries between the somites are once again

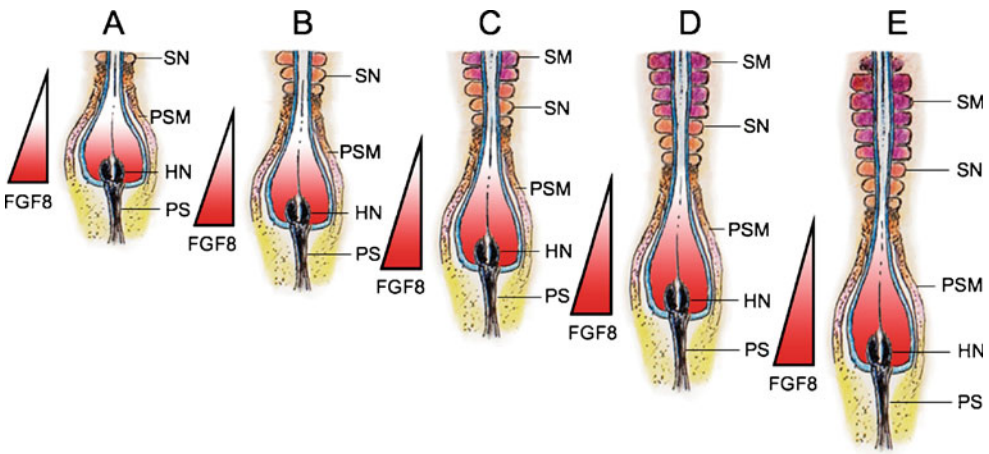

Fig. 8 *A–E* The molecular basis of the somitogenesis wavefront. Boundary formation at the PSM is linked to expressions of fibroblast growth factor genes, especially *fgf8*. High concentrations of FGF8 maintains PSM cells in a primitive mesenchymal state, but a low concentration of FGF8 permits PSM cells to form boundary during the segmentation clock peak. Thus, the epithelial transformation (into somites) of PSM cells is negatively regulated by *fgf8*. High concentration of FGF8 is expressed by newly formed PSM cells at Hensen's node, and low concentration is expressed in "older" PSM cells near the somitogenesis front. Thus, the limit between the high and low *fgf8* domains near the site of active somitogenesis represents the somitogenesis wavefront (represented by the apex of the FGF8 *triangle*). Because new PSM cells are continually being formed near Hensen nodes and the PSM column constantly elongates and gets ever "older" near the last formed somite, the wavefront also moves caudally. High concentration of FGF8 is indicated by *deep red colour* and low concentration by *pale grey* to *white*. The moving FGF8 gradient is also displayed by the *coloured triangle*. *HN* Hensen's node, *PS* primitive streak, *PSM* presomitic mesoderm, *SN* new somite, *SM* mature somite. Significance of somite colours as in Fig. 3

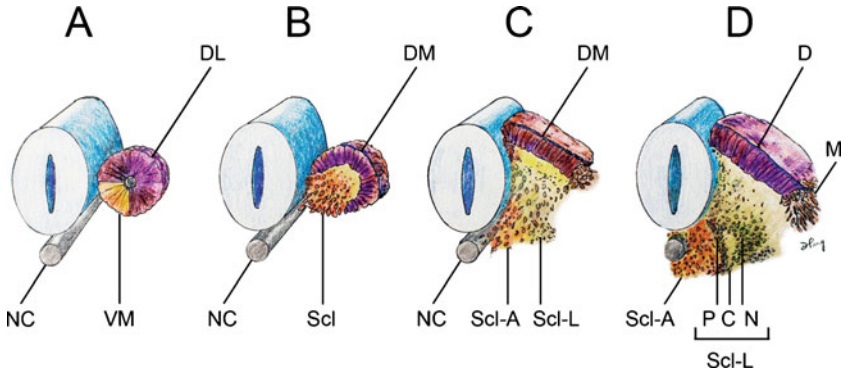

Fig. 9 Dorsoventral differentiation of somite. *A* Epithelial somite shows ventromedial cells (*VM*) destined to form the sclerotome. *B* Ventromedial sclerotome cells (*Scl*) de-epithelize from the somite and migrate towards the ventral notochord (*NC*). *C* Sclerotomal cells further subdivide into an axial cluster (*Scl-A*) surrounding the notochord, and lateral paired clusters (*Scl-L*) flanking the perichordal axial sclerotome. Dorsolateral somite retains its epithelial pattern to become the dermomyotome (*DM*). *D* The lateral sclerotome (*Scl-L*) forms a triangle next to the axial sclerotome. The three sides of the triangle become anlagen for the pedicle (*P*), neural arch (*N*) and the costal process (*C*), respectively. The dermomyotome also subdivides into the dermatome (*D*) and the lateral migrating myotome (*M*)

changed and "reshuffled" during the development of the sclerotome, so that the later boundaries between the vertebral bodies do not match up with the original intersomitic clefts [12].

During somitic differentiation, the ventromedial cells destined to become sclerotome subdivide into paired lateral clusters flanking the ventral aspects of the neural tube and an unpaired median (axial) cluster surrounding the midline notochord (Fig. 12). The formation of the vertebral column takes place first in the lateral sclerotome, where a conspicuous subdivision into a densely packed caudal half and a more loosely cellular cranial half soon appear, separated by a fissure (of von Ebner [91]). The loose cranial half attracts, promotes, and supports the growth and expansion of peripheral nervous tissue from the neural tube and neural crests, but itself never chondrifies into vertebral parts (Fig. 13, middle). In contrast, the caudal densely packed mesenchyme of the lateral scleroderm soon takes on a triangular shape. The side of the triangle facing the axial perichordal sclerotome, which will become the future vertebral body, gives rise to the pedicle. The side facing dorsolaterally away from the axial sclerotome forms rudiments of the neural arch; and the side of the triangle facing ventro-laterally becomes the costal process (Fig. 9 D).

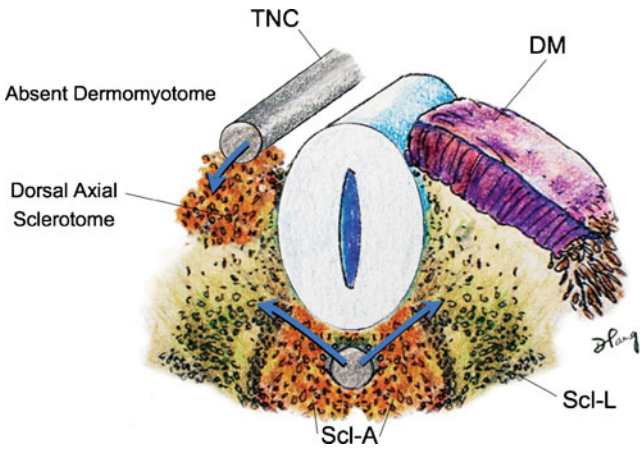

Fig. 10 A transplanted notochord (*TNC*) to the dorsal aspect of the somite induces sclerotomal differentiation dorsally and represses dermomyotomal formation on the side of the transplant, indicating inducers from the notochord directs dorsoventral specification of the somite. *DM* dermomyotome, *Scl-A* axial sclerotome, *Scl-L* lateral sclerotome

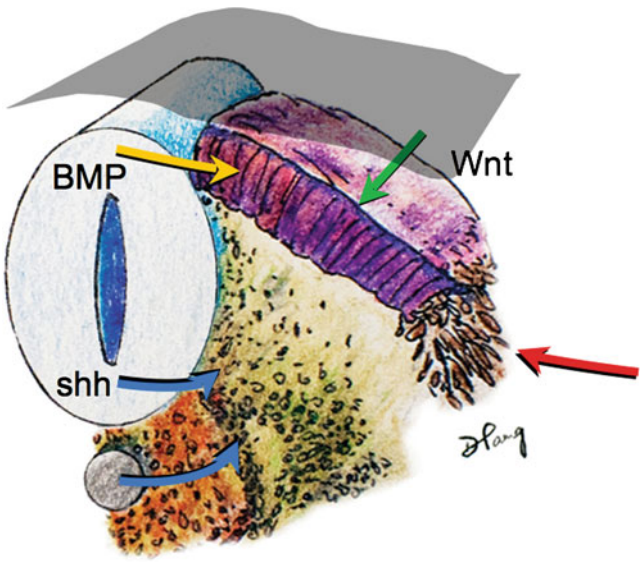

Fig. 11 Expressions of sonic hedgehog gene (shh) (*blue arrows*) from the notochord and floor plate of the neural tube signal sclerotomal differentiation and ventral migration from the somite. Bone morphogenetic protein (*BMP*) (*yellow arrow*) expressed by the roof plate and Wnt signalling (*green arrow*) from the ectoderm (*grey mantle*) induce dermomyotome differentiation. Other lateralizing signals (*red arrow*) further encourage myotomal cell development

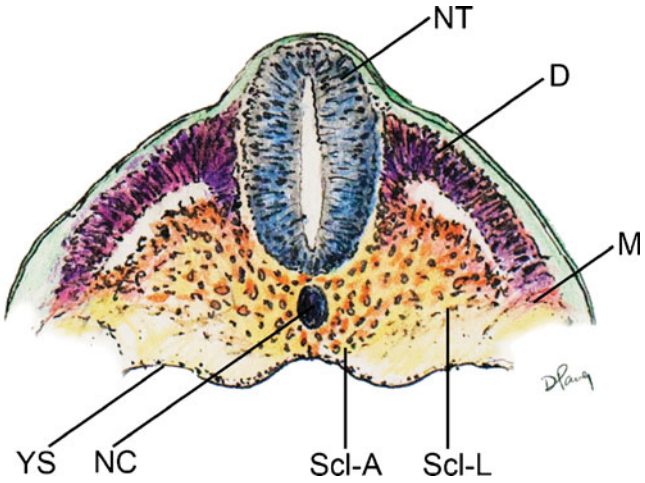

Fig. 12 Coronal section of chick embryo after dorsoventral differentiation of somites, showing axial or perichordal sclerotome (*Scl-A*) surrounding the notochord (*NC*), and lateral sclerotome (*Scl-L*) on both sides of the neural tube (*NT*). *D* dermatome, *M* myotome, *YS* yolk sac membrane

Shortly after the specifications of the lateral sclerotome into its arcual, costal, and pedicular components, the initially loosely meshed mesenchyme within the perichordal axial sclerotome also begins to show compartmentalization. A cell-dense zone develops at the same level as the dense caudal half of each lateral sclerotome, partly due to medial expansion of the lateral band of condensed tissues from the lateral sclerotome. The axial sclerotome in between these median dense zones remains loosely cellular. Later, the cranial-most layer of the axial dense zone, in line with von Ebner's fissure in the lateral sclerotome, becomes even more tightly packed and forms the intervertebral boundary zone (IBZ) (Fig. 13, middle). This intervertebral boundary mesenchyme ultimately forms the ring-like annulus fibrosus of the intervertebral disc, permanently enclosing a looser central core of nucleus pulposus made partly of notochordal remnants. The vertebral body itself is mainly made from chondrogenesis in the loose cell zone of the perichordal sclerotome, now called the prevertebra [11, 12, 24, 65], although contributions from the condensed tissue adjacent to the IBZ have been observed [16, 23]. As a final step, the pedicular anlagen from the lateral sclerotomes fuse with the chondrifying prevertebra of the axial sclerotome, whilst the neural arches surround the neural tube to complete the vertebral ring (Fig. 13, right). The costal component becomes the future transverse process but only in the thoracic region is it pre-destined to form ribs.

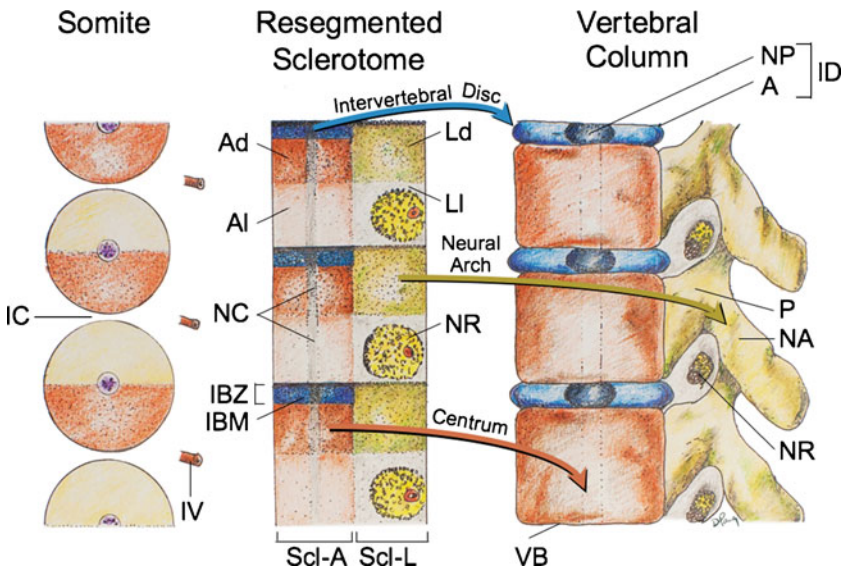

Fig. 13 Resegmentation of somites to form sclerotomes and changes of sclerotomal primordia to mature vertebral parts. The somitic and primordial origins of vertebral parts and phenotypic parts are colour-matched, and the locations of the somites, resegmented sclerotomes, and vertebrae along the embryonic axis are approximately counter-registered. During resegmentation, the sclerotome is formed from the caudal and rostral halves of two adjacent somites, such that the middle of the resegmented sclerotome lines up with the intersomitic cleft (*IC*). Both the axial sclerotome (*Scl-A*) and lateral sclerotome (*Scl-L*) develop dense and loose zones. The dense zone of the lateral sclerotome (*Ld*) becomes the neural arch (*NA*) and pedicle (*P*), which is attached to the rostral part of the vertebral body (*VB*) formed from chondrification of the loose (*Al*) and part of the dense zones (*Ad*) of the axial sclerotome. The rostral layer of the dense zone of the axial sclerotome soon forms the intervertebral boundary zone (*IBZ*) containing intervertebral boundary mesenchyme (*IBM*), which ultimately forms the annulus (*A*) and, together with notochord remnants (*NC*), the nucleus pulposus (*NP*) of the intervertebral disc (*ID*). The loose zone of the lateral sclerotome (*Ll*) does not form bone but promotes emergence of the nerve roots (*NR*). Thus, the neural arch is derived from a single somite but the vertebral body receives contributions from two adjacent somites. *IV* intersomitic vessel. *Arrows* indicate developmental fates of the sclerotomes

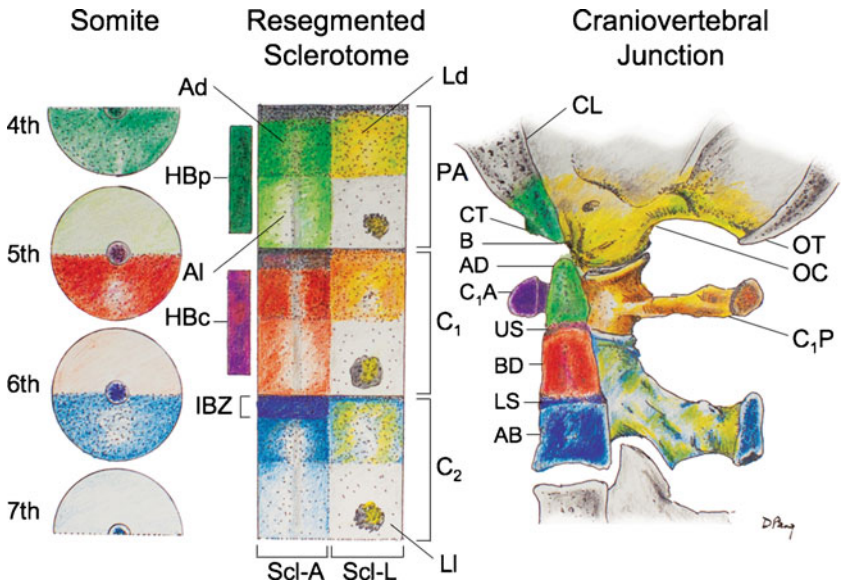

Fig. 14 Formation of the human craniovertebral junction. Sclerotomal primordia and their vertebral phenotypes are colour-matched. During resegmentation, the caudal half of the fourth somite (fourth occipital somite) and rostral half of the fifth somite combine to form the proatlas sclerotome (*PA*). Derived from the proatlas are: the axial zones (*Ad* and *Al*) which become the basion (*B*) of the basioccipital or clivus (*CL*) and the apical segment of the dens (*AD*); the lateral dense zone (*Ld*) becomes the exoccipital comprising the occipital condyle (*OC*), and lateral rim and opisthion (*OT*) of the foramen magnum; the proatlas' hypochordal bow (HB_p) forms the ventral clival tubercle (*CT*). The C_1 resegmented sclerotome (C_1) comes from adjacent halves of the fifth and sixth somites. Derived from the C_1 sclerotome are: the axial zones form the basal segment of the dens (*BD*); the lateral zone forms the posterior atlantal arch (C_1P); the hypochordal bow (HB_c) forms the anterior atlantal arch (C_1A). The C_2 resegmented sclerotome (C_2) comes from the sixth and seventh somites. From the C_2 sclerotome: the axial zone forms the C_2 vertebral body (*AB*); the lateral zone forms the neural arch of C_2 vertebra. The intervertebral boundary zone (*IBZ*) between the proatlas and C_1 sclerotome forms the upper dental synchondrosis (*US*) and the IBZ between the C_1 and C_2 sclerotomes forms the lower dental synchondrosis (*LS*)

Thus, the neural arch of the vertebra is derived from the caudal-lateral part of a single somite [16]. However, labelling and transplantation experiments of half-somites have repeatedly demonstrated that each vertebral body is made up of cells from the axial zones of two adjacent somites [2, 3]. Although the exact boundary of individual somite participation is not known [12], the juxta-positioning of axial and lateral sclerotomal components

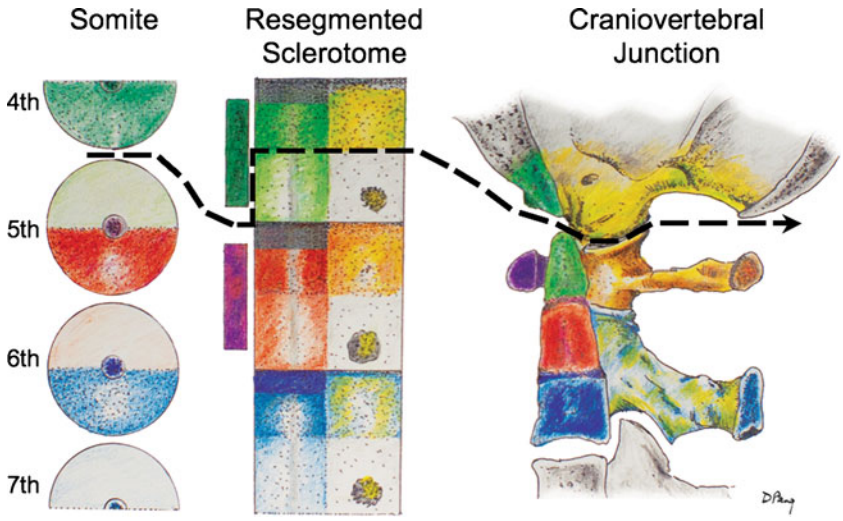

Fig. 15 The severance *line*, which results in final cellular separation of the skull from the cervical spine, runs through the original resegmentation fronts of the adjacent somites 4 and 5, corresponding to the junction between the basion and apical segment of the dens in the axial proatlas, and between the exoccipital, or future occipital condyle, and the lateral mass of C_1, derived from the lateral portion of the C_1 resegmented sclerotome

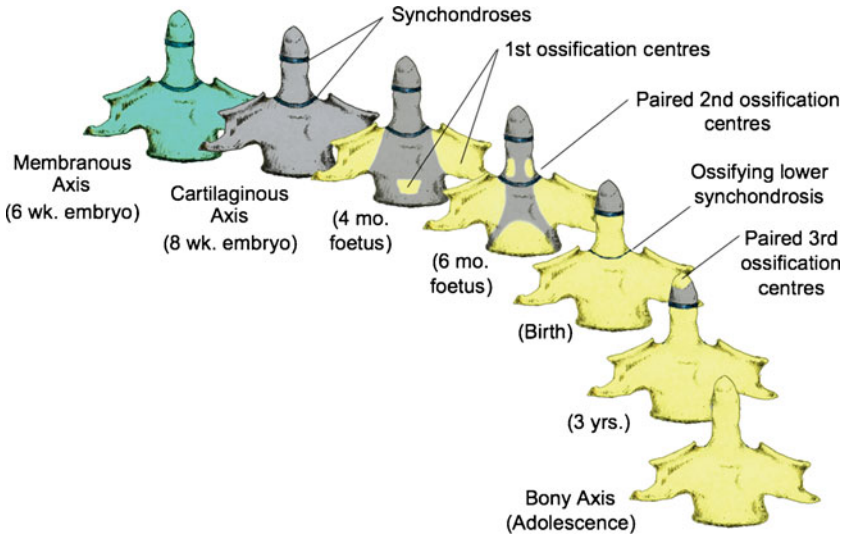

Fig. 16 The three developmental phases of the axis (C_2) and the three waves of ossification. The primordia for the dens components are assembled during the membranous phase. Upper and lower dental synchondroses are shown as *dense lines*. First wave of ossification at fourth foetal month consists of bilateral centres for the neural arches and a single centre for the centrum. Second wave at sixth foetal month consists of bilateral ossification centres for the basal dental segment. At birth, the basal dental centres should have integrated in the midline and begun to be fused to the centrum. Third wave of C_2 ossification occurs from 3 to 5 years post-natal life at the apical dental segment, which does not become fused to the basal dens till the 6–9th year, and fully formed during adolescence

suggests that each vertebra probably comes from the caudal half of one somite and the rostral half of the somite below [65]. This will explain the slightly off-step registration between the levels of the somite and the resegmented sclerotome [12, 17, 65] on the embryonic axis such that the middle of the resegmented sclerotome lines up with the original intersomitic cleft (Fig. 13, left and middle). Also, since the dense portion of the lateral sclerotome is in line with the dense zone of the axial sclerotome adjacent to the IBZ, it makes perfect sense that the mature pedicle is joined to the cranial and not the caudal half of the vertebral body [12]. It also follows that the spinal nerve, ganglion, and blood vessel from the corresponding somitic segment, being associated with the loose cranial half of the lateral sclerotome, must cross above its own neural arch, and that the corresponding segment of the spinal cord is always slightly more rostral to its companion vertebral body (Fig. 13, right). Given that there are eight cervical somites but only seven resegmented axial sclerotomes and consequently seven cervical vertebrae, the C_1 nerve root emerges above the C_1 neural arch and the C_8 nerve root comes through below the C_7 neural arch and above the T_1 neural arch, which in fact is derived from the C_8 somite. Finally, resegmentation of the sclerotome explains why the original "pre-resegmented" intersomitic vessel ultimately enters the mid-

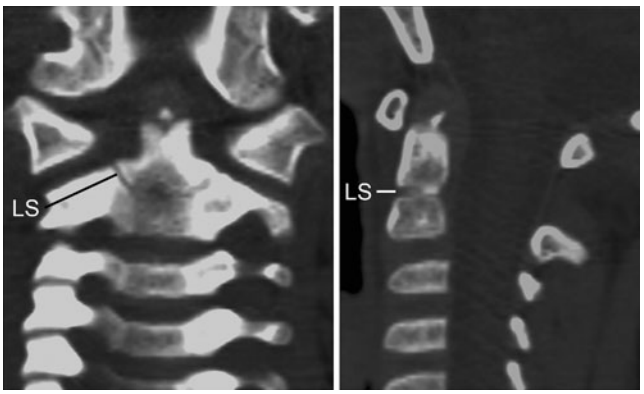

Fig. 17 State of ossification of the dens of a 4-year-old child. The tip of the basal dental segment is bicornuate from bilateral secondary ossification centres. Small density above this represents early third wave of ossification within the apical dental segment. Note lower dental synchondrosis (*LS*) in the coronal and sagittal views

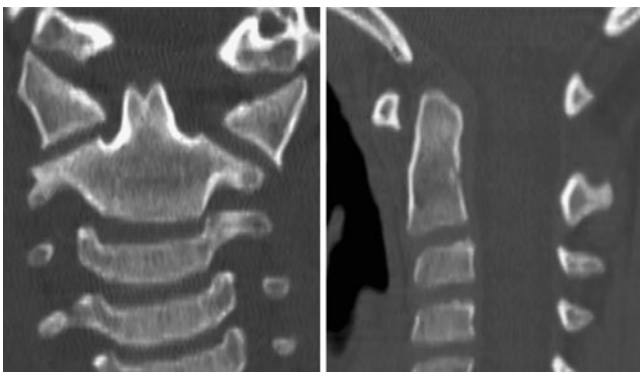

Fig. 18 Dens bicornis in a 7-year-old child. Lower synchondrosis has closed. Dens pivot is of normal height, suggesting the bifid tip is of the apical segment

point of the vertebral body as the segmental nutrient artery.

Special developmental features of the CVJ

The CVJ is the product of the occipital somites and the first three cervical somites. There is controversy regarding the proper number of occipital somites in vertebrates. Wilting et al. and others [14, 78, 99] thought that there were five occipital somites in chick and mouse but conceded that the first somite either disappeared early or was an insignificant clan of cells that lacked sclerotomal lineage. Müller and O'Rahilly [65] studied staged human embryos and concluded that, in humans, there are only four occipital somites that participate in the formation of the skull base. The transitional zone between the skull and the cervical spine is thus taken to be between the fourth and fifth somites. During the fourth week of gestation, there are consequently 4 occipital, 8 cervical, 12 thoracic, 5 lumbar, 5 sacral, and 8 to 10 coccygeal somites, 42 pairs all told.

Occipital somites (somites 1–4) and the proatlas

Following the general schema, the first three occipital somites give rise to an axial perichordal sclerotome and a lateral sclerotome, but no resegmentation takes place here. The axial sclerotomes never subdivide into dense and loose zones and therefore no intervertebral boundary mesenchyme exists. They all eventually fuse into a unit which later chondrifies to become the rostral basioccipital [65]. The first three lateral occipital sclerotomes, like the vertebral sclerotomes, form dense and loose zones, and the loose zones of the second and third lateral occipital sclerotomes foster expansion of the upper and lower hypoglossal nerve roots and artery, whilst the corresponding dense zones form the bony hypoglossal canal.

Unlike the first three occipital somites, the fourth occipital (O_4) somite does show resegmentation. Its caudal dense zone combines with the cranial loose half of the first cervical somite to produce the transitional sclerotome called the proatlas [17, 51, 59, 60, 64, 65] (Fig. 14, left and

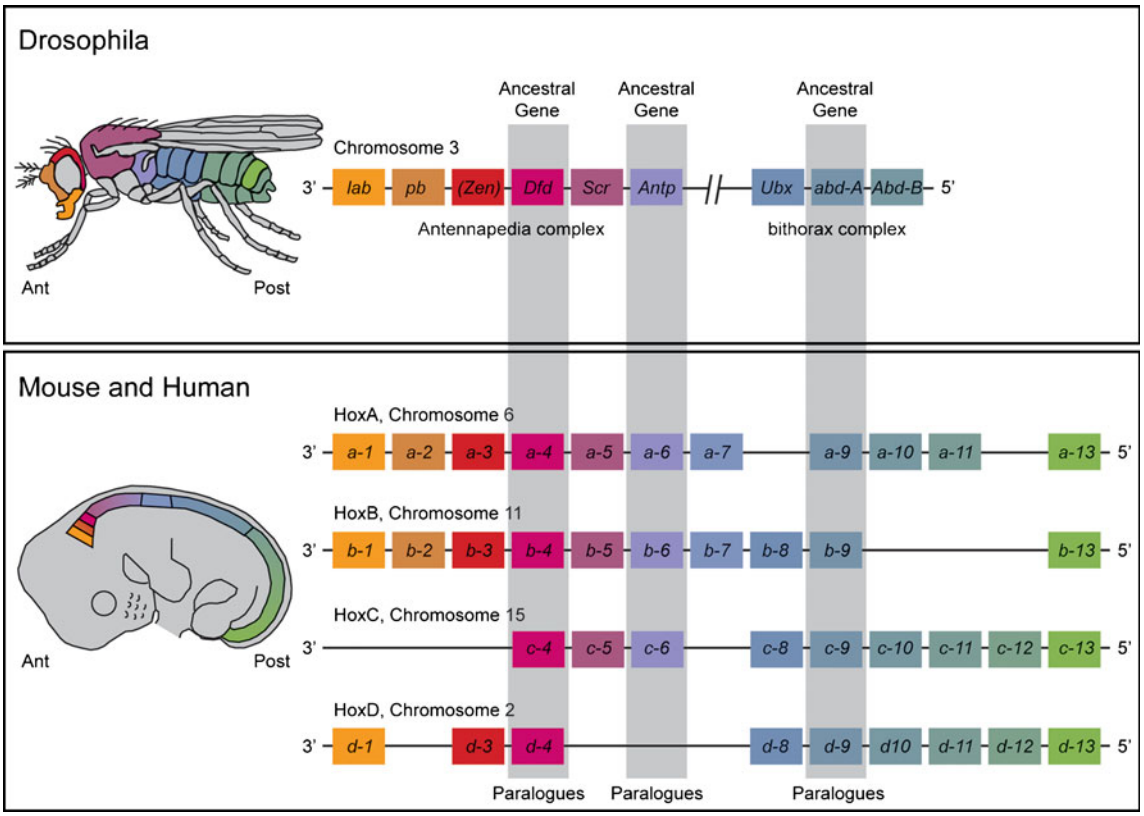

Fig. 19 Hox genes in mouse and human with their phylogenetic counterparts in *Drosophila*; 39 Hox genes are involved in the mouse and human vertebral column, found in four clusters of Hox A, B, C and D on four chromosomes (6, 11, 15 and 2), designated by *Arabic numbers* within each cluster and arranged as paralogues, so that the lower numbered Hox paralogues such as *Hox a-1* and *Hox d-1* are located on the anterior 3′ position of the chromosomes, and the higher numbered paralogues such as *Hox a-13* and *Hox d-13* are on the 5′ posterior position of the chromosomes. There is also temporal and structural colinearity with the embryonic axis so that the lower numbered paralogues are expressed earlier and more anterior on the embryonic axis than the higher numbered paralogues. (See colour match between genes and their expression domains on the embryonic axis.) Three sets of paralogues and their corresponding ancestral genes are designated by the *grey bars*

middle). The cranial region of the axial sclerotome of the proatlas soon fuses with the other three axial occipital sclerotomes to become the basion of the basioccipital [64], but its most caudal portion, probably derived from the first cervical somite (somite 5), forms the anlage for the apical segment of the dens. Late in resegmentation, a boundary zone appears between this apical dental centrum and the loosely cellular prevertebra of the basioccipital, and the former soon detaches from the basioccipital and eventually becomes joined to the basal segment of the dens to complete the dental pivot (see below) [65, 99] (Fig. 14). Herein lies the most unique feature of the transitional zone of the CVJ between somites 4 and 5: unlike other IBZs that form intervertebral discs, downstream activity of the proatlas' IBZ includes a physical severance of cells from the immediately adjacent loose perichordal zone of the basioccipital. The severance line appears to go through the original resegmentation fronts of the adjacent somites 4 and 5, so that the final cellular separation occurs right through the junction between the basion and the apical segment of the dens, both derived from the axial portion of the proatlas, which in turn comes from a combination of the caudal half of somite 4 and the rostral half of somite 5 (Fig. 15). This action, no doubt mediated by special cleavage genes, not only allows the skull to become independent from the vertebral column, but also the separation of the primordium for the apical dens from the basiocciput and final installation of the axis–dens assembly.

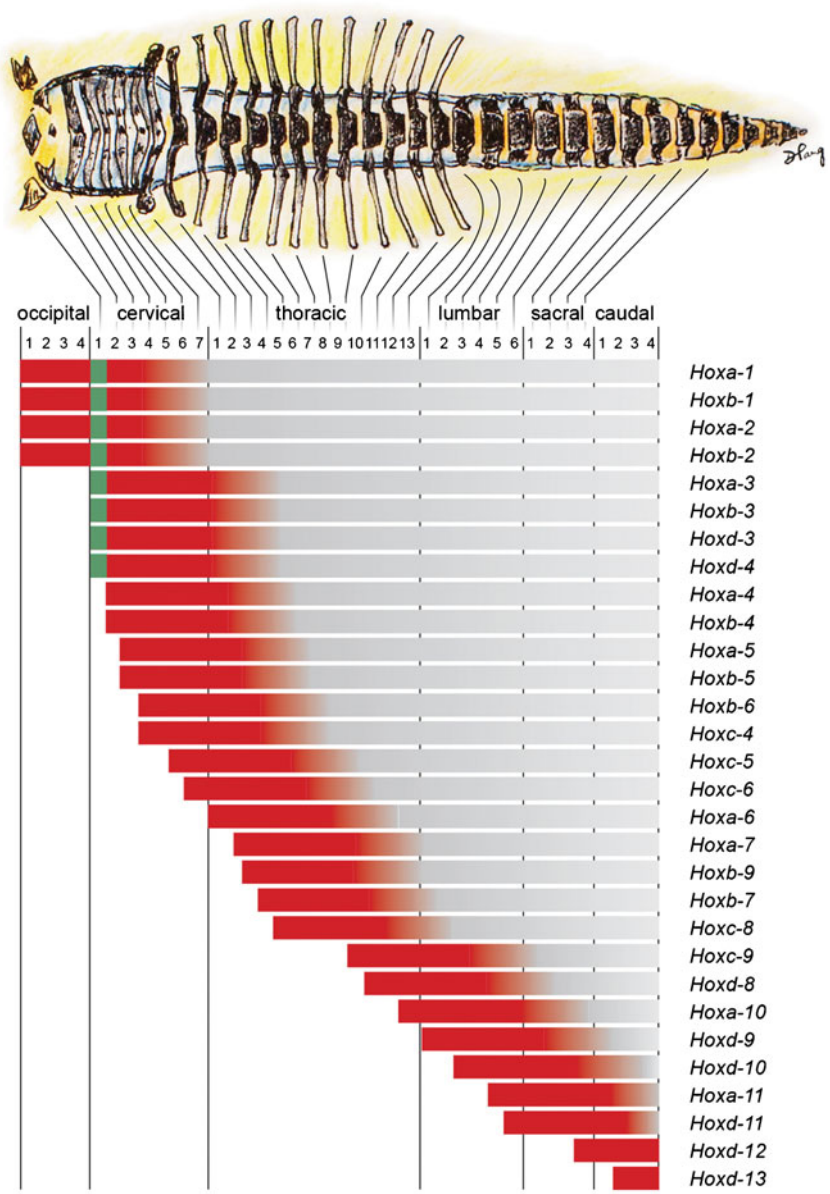

Fig. 20 Expression domains of *Hox* genes lined up with the mouse embryonic vertebral column. Only the anterior expression boundary (in *red*) is important, and since multiple genes have the same anterior expression boundary along the prevertebral axis, each prevertebral segment has its own combination of *Hox* gene expression domains (Hox code). For example, the Hox code for C_1 is Hox *a-1*, *b-1*, *a-2*, *b-2*, *a-3*, *b-3*, *d-3* and *d-4* (designated by the vertical *green bar*)

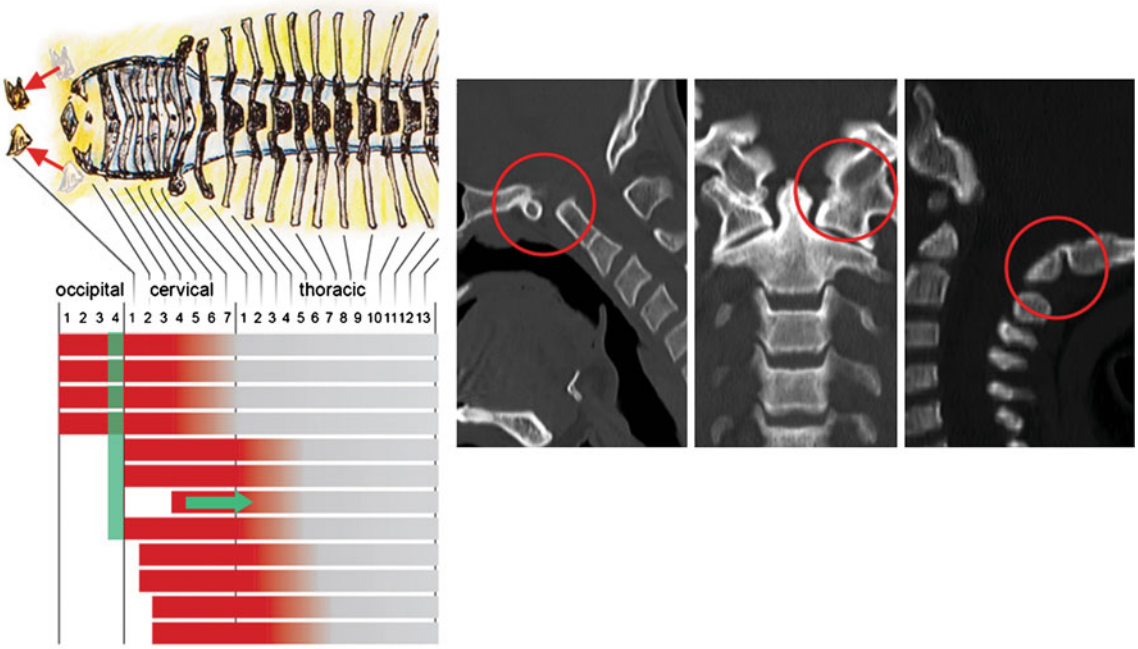

Fig. 21 Anterior homeotic transformation. Mutation of the Hox d-3 gene in the mouse causes a caudal recession of its anterior expression domain (*green arrow*), allowing the Hox code of the C_1 segment (*green bar*) to resemble that of an occipital somite (Note *green bar* representing C_1 Hox Code has moved up to occipital sclerotome position). This renders the C_1 sclerotome to "behave" like an occipital segment (symbolised in the figure by rostral movements of the C_1 sclerotomes to a cranial position; see *red arrows*) and the anterior and posterior arches of C_1 become fused to the basioccipital and exoccipital. *Inset* shows the human version of anterior homeotic transformation with assimilation of C_1 to the occiput

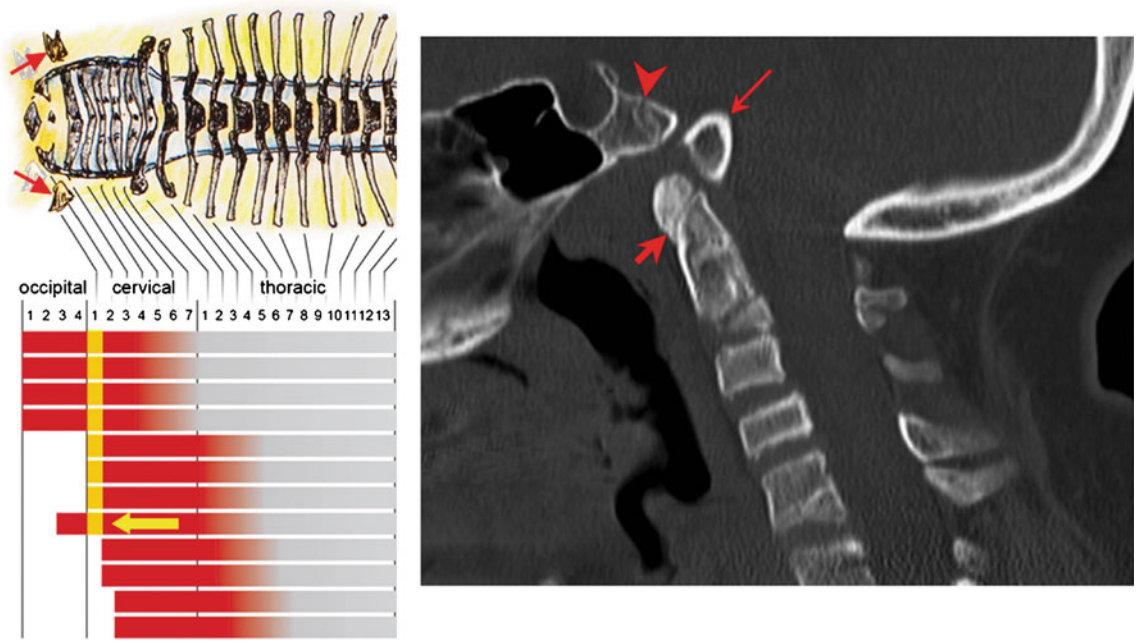

Fig. 22 Posterior homeotic transformation. "Gain-of-function" mutation of the murine Hox d-4 gene causes its anterior expression domain to extend cranially (*yellow arrow*), allowing the Hox code for the O_4 segment (*yellow bar*) to resemble that of the C_1 and C_2 sclerotomes (*yellow bar* moved to C_1 Hox code position) and render the basiocciput to "imitate" the C_1 segment (symbolised in the figure by caudal movement of the C_1 sclerotomes; see *red arrows* on the drawing). The *inset* shows the human version of posterior homeotic transformation: the basion (*long arrow*) is detached from the upper clivus (*arrow head*), and the C_1 anterior arch (*short arrow*) is fused to the apical dens as if C_1 is trying to become C_2 by acquiring a "true centrum"

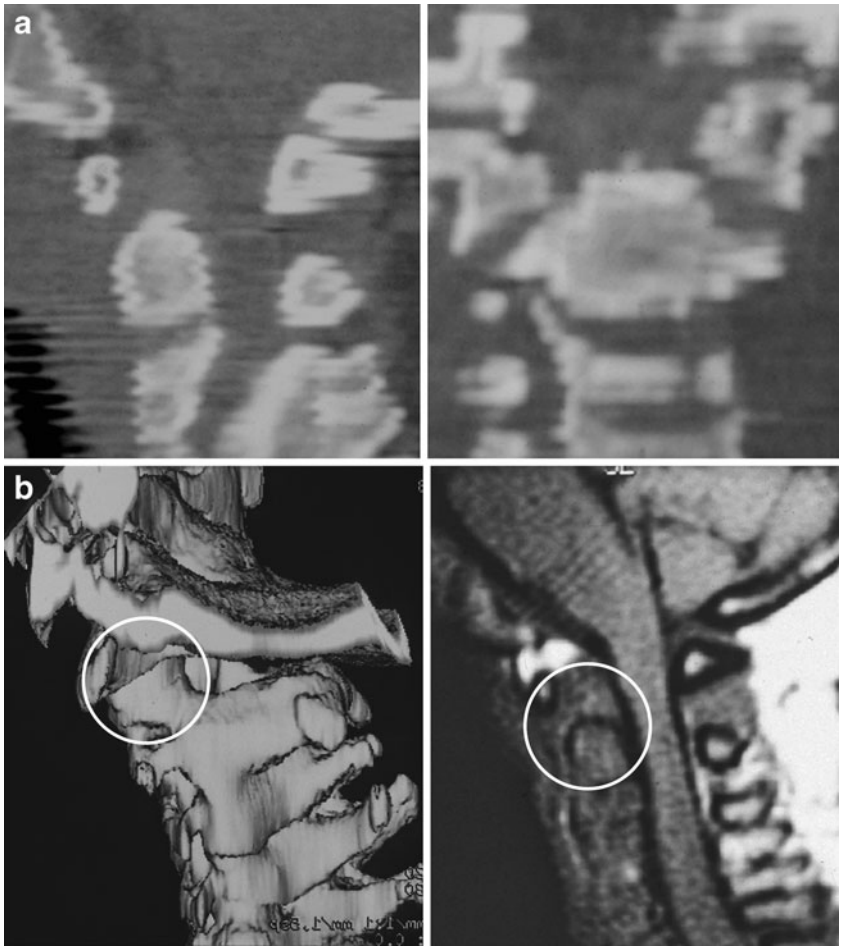

Fig. 23 Complete agenesis of the dens in a 10-year-old child with spondyloepiphyseal dysplasia. **a** CT sagittal and coronal views show no dental pivot although the centrum with a flat top does rise up above the "expected" level of the lower dental synchondrosis. **b** 3-D CT reconstruction and MR show the flat top of the centrum and potential for instability

Fig. 24 Agenesis of basal dental segment with a stumpy C_2 centrum and a high-riding "floating" apical ossiculum (*between arrows*)

Fig. 25 Agenesis of apical dental segment, with a slightly short dental pivot but a definite basal segment (*pointed*) and a lower dental synchondrosis (*LS*). *Arrow* points to anterior arch of C_1. Note platybasia and Chiari I malformation

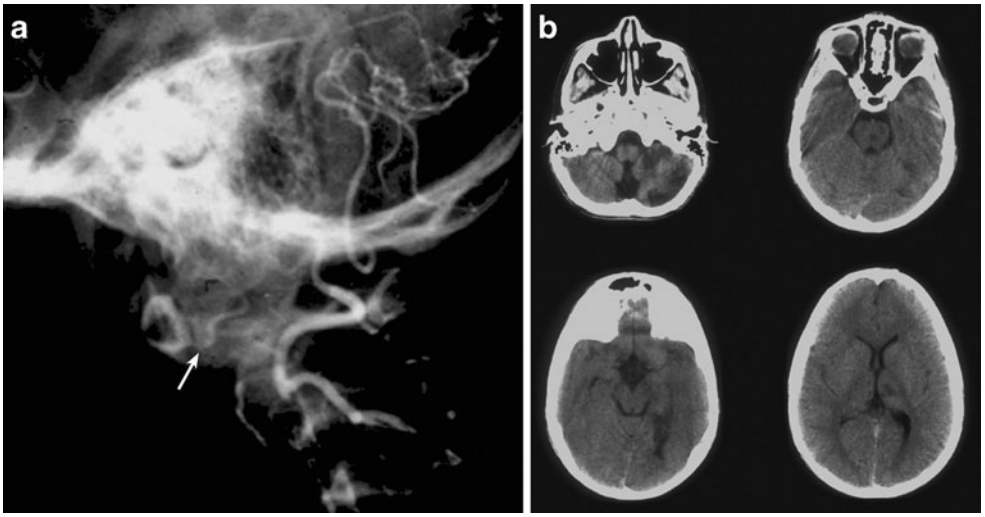

Fig. 26 Os odontoideum in an 8-year-old child presented with multiple cerebellar and thalamic strokes. **a** Cerebral angiogram shows os odontoideum with a corrugated horn-like inferior edge (*arrow*) with anterior C_1–C_2 subluxation and stretch injury to the vertebral artery. **b** CT scans show multiple small infarcts of left cerebellar hemisphere and thalamus secondary to multiple vertebrobasilar emboli

The lateral dense region of the proatlas becomes the two exoccipitals, which later form the two occipital condyles and the remainder of the anterolateral rim of the foramen magnum (Fig. 14). The lateral loose region promotes emergence of the C_1 nerve root. In humans, an additional arcuate cluster of dense proatlas cells ventral to the notochord, aptly called the hypochordal bow, gives rise to the bony anterior clival tubercle on the ventral surface of the basioccipital [64, 65] (Fig. 14).

First three cervical somites (somites 5–7)

Axial sclerotomes During resegmentation, the caudal half of somite 5 and the cranial half of somite 6 combine to produce the first cervical sclerotome; likewise, the second cervical sclerotome is made up of corresponding parts of somites 6 and 7. In the axial region of these sclerotomes destined to form vertebral centra, dense and loose zones appear in regular succession as in the lower cervical sclerotomes. The loose prevertebral zone of the first cervical sclerotome gives rise to the basal segment of the dens, and that of the second cervical sclerotome becomes the body of the axis (Fig. 14). Unlike in the more caudal sclerotomes, however, where the dense IBZ ultimately becomes the annulus and nucleus pulposus of an intervertebral disc, the dense zones in the first two cervical sclerotomes do not form true intervertebral discs and soon disappear [65]. Their intervertebral boundary mesenchyme gradually turns into the upper and lower dental synchondroses that ultimately cement the apical to the basal dens and the basal dens to the body of C_2, respectively (Fig. 14).

Thus after resegmentation, the human membranous axis consists of three median constituents that have been designated the apical dental segment from the caudal proatlas, the basal dental segment from the first cervical sclerotome, and the body of the axis from the second cervical sclerotome [6, 7, 36, 78, 82]. These three constituents chondrify simultaneously around 6 weeks of gestation but remain segregated by the more cellular upper and lower dental synchondroses. Ossification of the cartilaginous axis occurs in three chronological waves (Fig. 16). The first wave appears as a single ossification centre within the axial body around 4 months of gestation. The second wave begins at 6 months of gestation as two separate ossification centres on each side of the basal dental segment [69, 75, 95, 100]. At birth, these two centres integrate and fuse, and the main component of the dens should at least have begun to show bony fusion with the axis body, even though a clear rarification may still be discernible at the lower synchondrosis till the fifth or sixth post-natal year (Figs. 16 and 17).

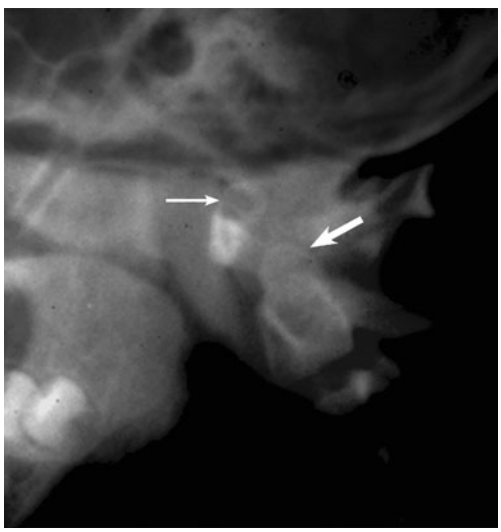

Fig. 27 Ossiculum terminale persistens (*thin arrow*), detached from the slightly shortened dental pivot formed by the basal dental segment (*thick arrow*)

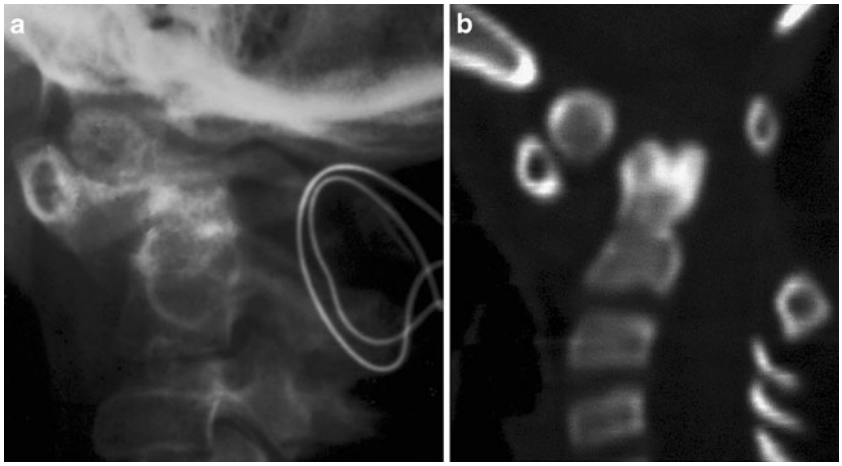

Fig. 28 Unstable os odontoideum with C_1–C_2 subluxation. **a** Widened ADI (13 mm) and a failed posterior C_1–C_2 fusion. **b** Another os with tall but jagged remaining dental pivot suggesting a traumatic aetiology

Occasionally, the basal dens remains bifid (dens bicornis) when the third wave of ossification arrives within the apical dens around 3 to 5 years of age [6, 53, 75] (Figs. 16, 17, and 18). Ossification of the dental tip and bony fusion of the upper synchondrosis are not completed until adolescence [55, 56, 94, 96].

Lastly, the apical ligament is almost certainly derived from the axial proatlas, and the alar and transverse atlantal

Fig. 29 Unstable ossiculum terminale in a 2-year-old child with intermittent quadriparesis. **a** Flexion (*upper*) and extension (*lower*) sagittal reconstructed CTs showing highly mobile ossiculum (*O*) and C_1 with obvious translational subluxation. **b** Sagittal T_2 MRI shows C_1 cord compression and T_2 signal changes in the cord. **c** Post-operative sagittal CT (*left*) and MRI (*right*) showing resection of C_1 posterior arch, reduced C_1–C_2 subluxation after bone grafts (*G*) and inside–outside screw plate occipital–C_2–C_3 fusion. MRI (*right*) shows restored width of the upper cervical canal and relief of cord compression. *O* ossiculum terminale, *C_1* anterior arch of C_1

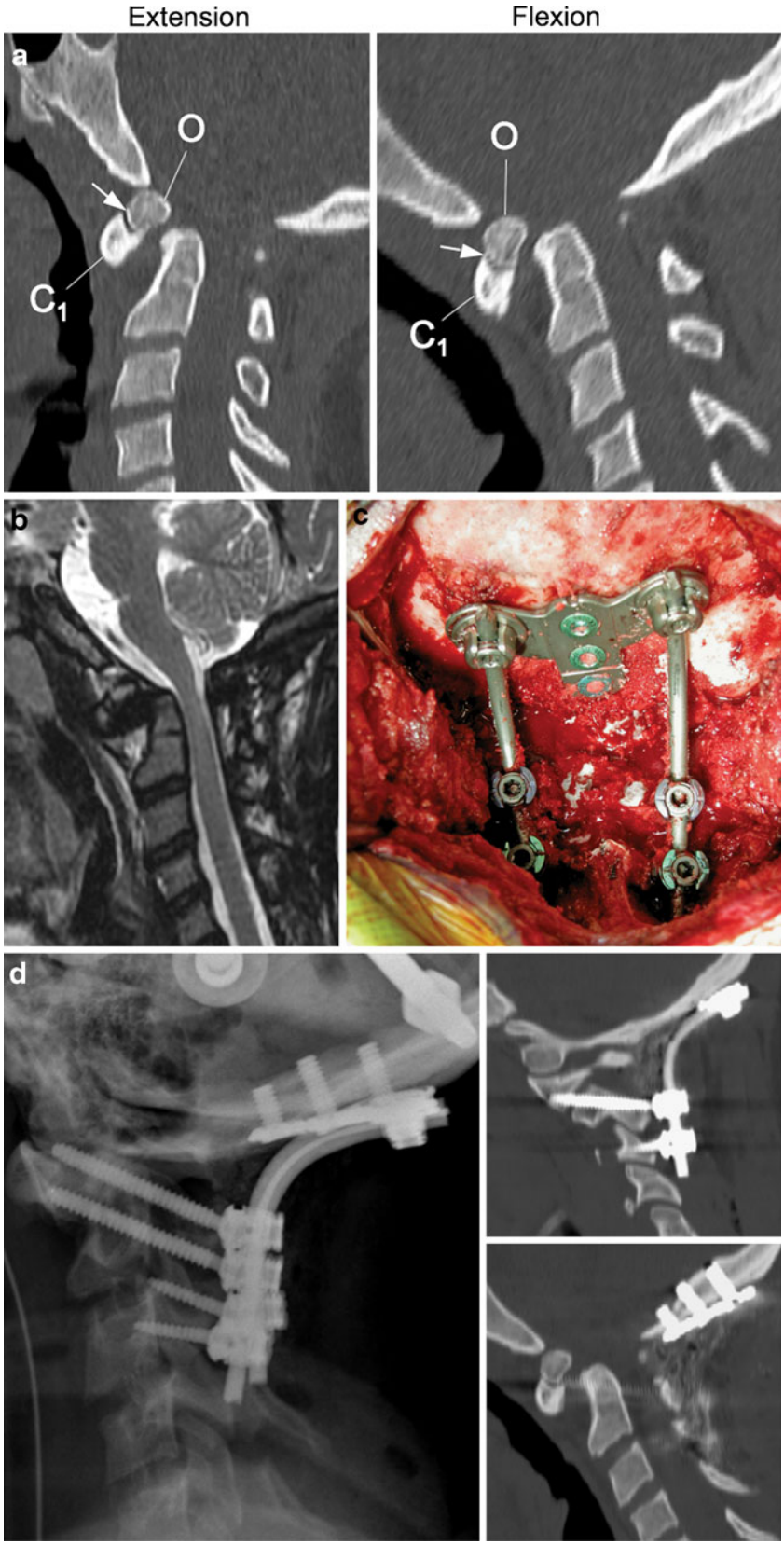

Fig. 30 Case 1: 10-year-old boy with ossiculum terminale. **a** Flexion–extension CT shows highly mobile ossiculum and anterior subluxation. The ossiculum terminale (*O*) forms a joint (*arrow*) with the posterior surface of the anterior arch of C_1 (C_1). Both C_1 and ossiculum move together as one unit. **b** Sagittal MR in neutral position shows narrowing of upper cervical canal. **c** After maximum intraoperative reduction and partial resection of the C_1 posterior arch, the occiput is fused to C_2 and C_3 using a screw plate and contoured upright rods. **d** Post-operative plain film (*left side*) and CTs (*right side*) show the C_2 transarticular screws to include the lateral mass of C_1 and the C_3 lateral mass screws. Note the three occipital screws through the thick mid-occipital keel for the occipital plate

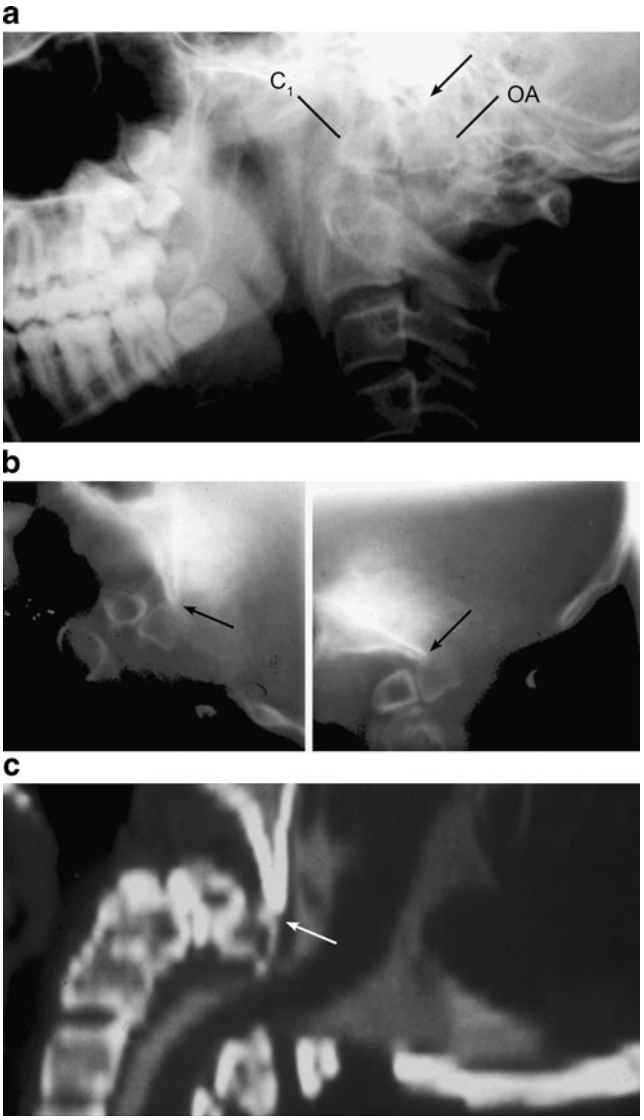

Fig. 31 Os avis with severe posterior subluxation of skull and C_1 on C_2 producing quadriparesis. **a** The bone directly above the dental pivot is in fact a posteriorly shifted C_1 anterior arch (*C_1*). The os avis (*OA*) is just behind the C_1 arch and is attached to the clivus marked by the *arrow*. Note posteriorly shifted posterior arch of C_1. **b** Flexion–extension polytomography shows relationship between C_1 arch, clivus and os avis. Note attachment of the os with the clivus tip (*arrow*) and the unchanging (*fixed*) relationship with the clivus during flexion and extension. **c** CT myelogram shows spinal cord compression by the os avis during extension. *Arrow* marks attachment of os avis to clival tip

ligaments are from the axial component of the first cervical sclerotome in association with the basal dental segments [65].

Lateral sclerotomes The lateral dense zone of the first cervical sclerotome develops into the posterior arch of the atlas, whilst the lateral dense zone of the second cervical sclerotome forms the arch of the axis. Their respective loose zones promote outgrowths of the second and third cervical nerves and segmental arteries. The hypochordal bow of the first cervical sclerotome ventral to the notochord subsequently forms the anterior arch of the atlas (Fig. 14, middle and right) [63–65, 82]. No definite hypochordal bows are seen caudal to this level and equivalent cells in the lower segments appear to play no role in the formation of the vertebral column.

Genetic control of CVJ development

Hox genes: the control of rostrocaudal specification

Following primary segmentation, the determination of the positional identity of the prevertebral segments along the embryonic axis, which in turn ordains the regional developmental specifications of the vertebral phenotypes, is controlled by Hox genes. The mammalian Hox genes encode transcription factors used in regulating the establishment of the body plan. They contain the phylogenetically highly conserved homeobox domain [24, 42, 43]. In mouse and humans, there are 39 Hox genes distributed in four linkage clusters, Hox A, B, C, and D, on four different chromosomes (chromosomes 6, 11, 15, and 2) (Fig. 19). The members of each cluster, designated by Arabic numerals, are also grouped vertically along the clusters because analogous members of each group are linked by common origin from a single ancestral gene, so that *Hox* a_4, b_4, c_4, and d_4 are connected to the same phylogenetic origin and are called paralogues (Fig. 19). The lower numbered paralogues are located on the anterior 3′ axis of the chromosome and the higher numbered ones are on its posterior 5′ locations (Fig. 19).

Hox genes are expressed in mesodermal and ectodermal cells along the body axis. Each gene has a characteristic and distinct anterior boundary of expres-

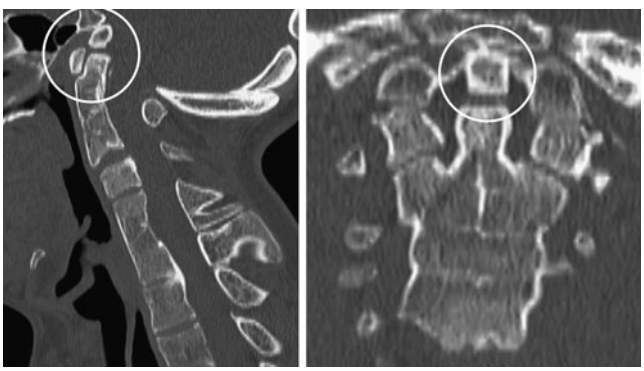

Fig. 32 Undescended apical dens still fused to the clivus (os avis). The dental pivot has a flat top but tall enough for the TAL and has no instability. Other anomalies such as multiple vertebral centra fusion, basilar invagination of the opisthion and stenosis by C_1 posterior arch cause compressive myelopathy

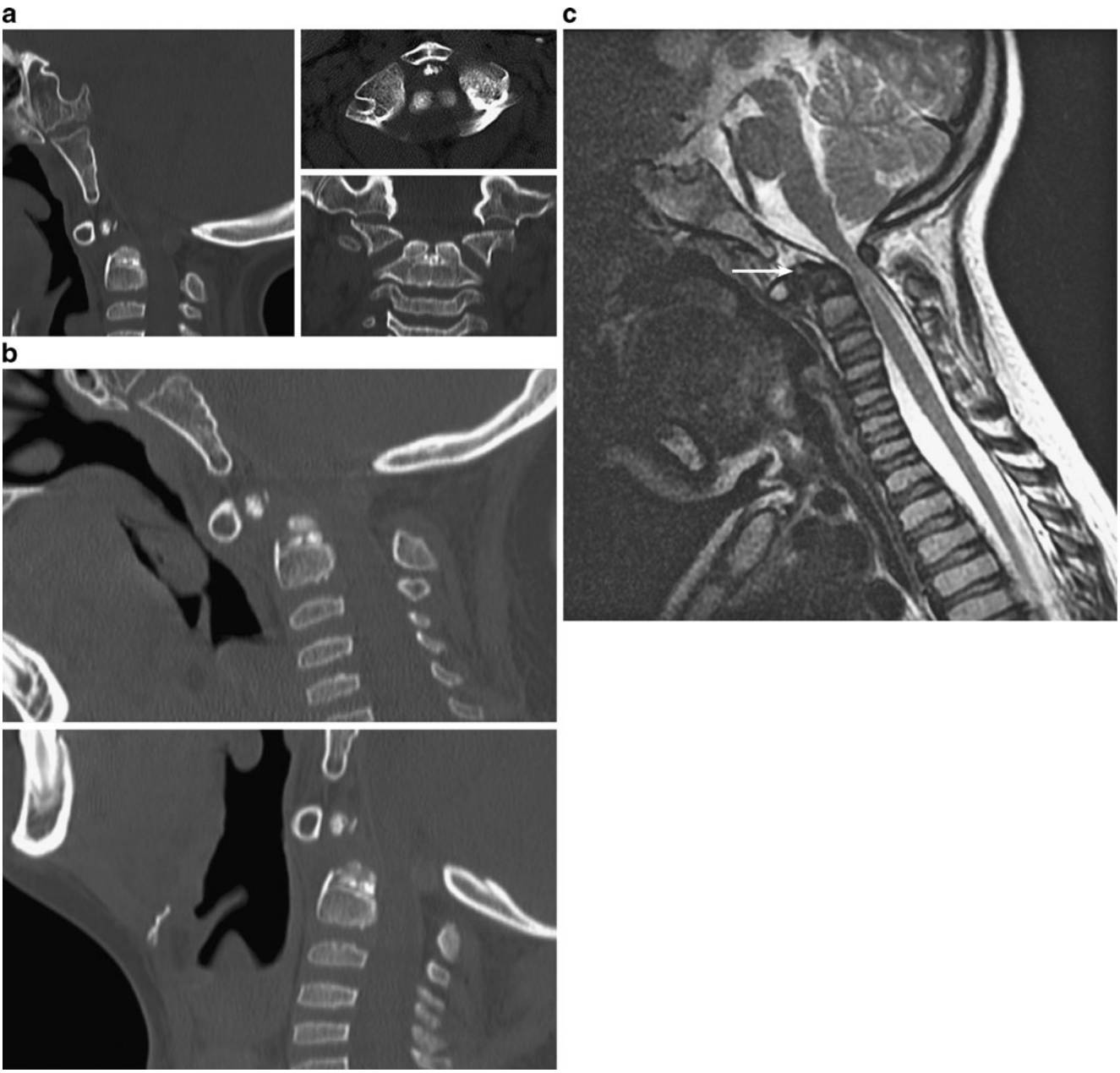

Fig. 33 Completely bifid dens. **a** Note complete lack of midline integration of basal dental segment down to lower dental synchondrosis and an unfused and forward dislocated apical dens, suggesting midline integration abnormality interferes with growth and fusion of adjacent upper dental synchondrosis. **b** Flexion–extension CT shows C_1–C_2 instability. **c** Sagittal MR shows severe cord compression with flexion. *Arrow* points to small ossiculum

sion. A temporal and structural colinearity exists between the position of a gene in a cluster and its expression pattern. Thus, genes from the more anterior 3′ locations in the Hox clusters are expressed earlier and always occupy more anterior (cranial) expression domains than genes closer to the posterior 5′ location in the clusters (Fig. 19). For example, *Hox a-3* has a more anterior expression domain than *Hox a-9* and similarly between *Hox d-4* and *Hox d-10*.

Functionally, only the anterior boundary of the Hox expression is important. Since multiple genes have the same anterior expression boundary along the prevertebral axis, each metameric segment can be identified by its own characteristic combination of Hox gene expression domains, i.e. its own Hox code (Fig. 20). A specific Hox code acts as a master switch in determining the exact positional identity of a mesodermal segment along the body axis, and via regional idiosyncrasies in development, the

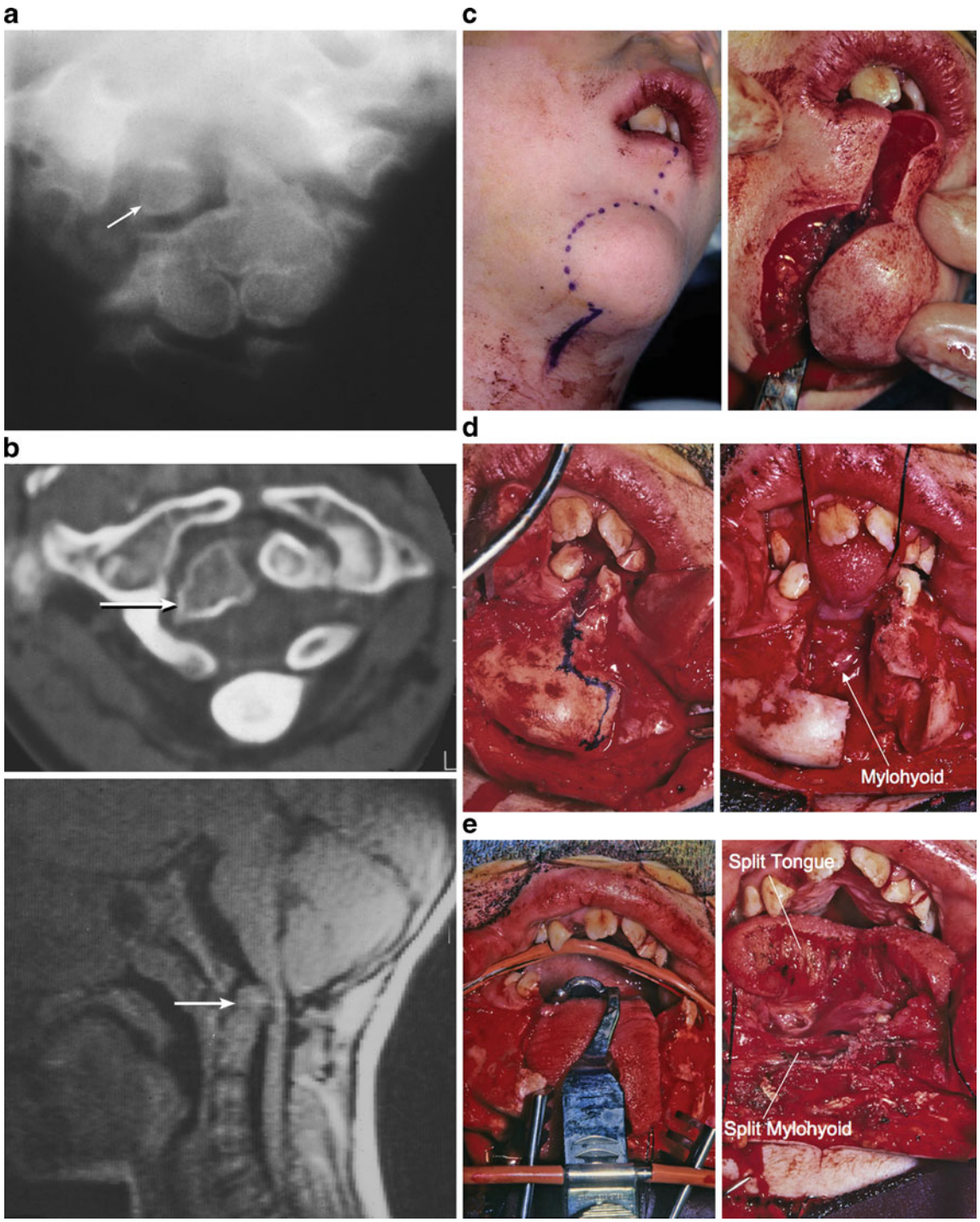

Fig. 34 Illustrative case 2: 6-year-old boy with absent midline integration of basal dental segment. **a** Non-fusion of right "hemi-os" to the C_2 centrum suggests interference with adjacent dental synchondrosis fusion. Note bifid C_3 centrum and fusion of C_2 and C_3 centra. **b** Floating hemi-os (*arrow*) on the axial CT (*left*) and backward "popping" of the hemi-os with cord compression on MRI (*right*). **c** Incision for midline mandibulotomy. **d** Step osteotomy of midline mandibulotomy for perfect re-attachment. **e** *Left*: difficulty in exposing the posterior pharynx even after mandibulotomy. *Right*: both the tongue and part of the mylohyoid have to be split in the middle to expose the posterior pharynx. **f** *Left*: exposure of the posterior pharynx after splitting the soft palate. *Right*: exposure of the anterior C_1 arch after incising the pharyngeal mucosa. **g** Odontoid resection. *Left*: subperiosteal exposure of the C_1 anterior arch. *Middle*: after drilling off the middle portion of the C_1 arch, the floating hemi-os is exposed. The fixed left hemi-os has been partially removed. *Right*: after removal of both the floating and fixed hemi-os, the transverse atlantal ligament (*TAL*) is exposed. **h** Post-operative axial CT showing complete removal of the mobile right hemi-os and most of the fixed hemi-os on the left

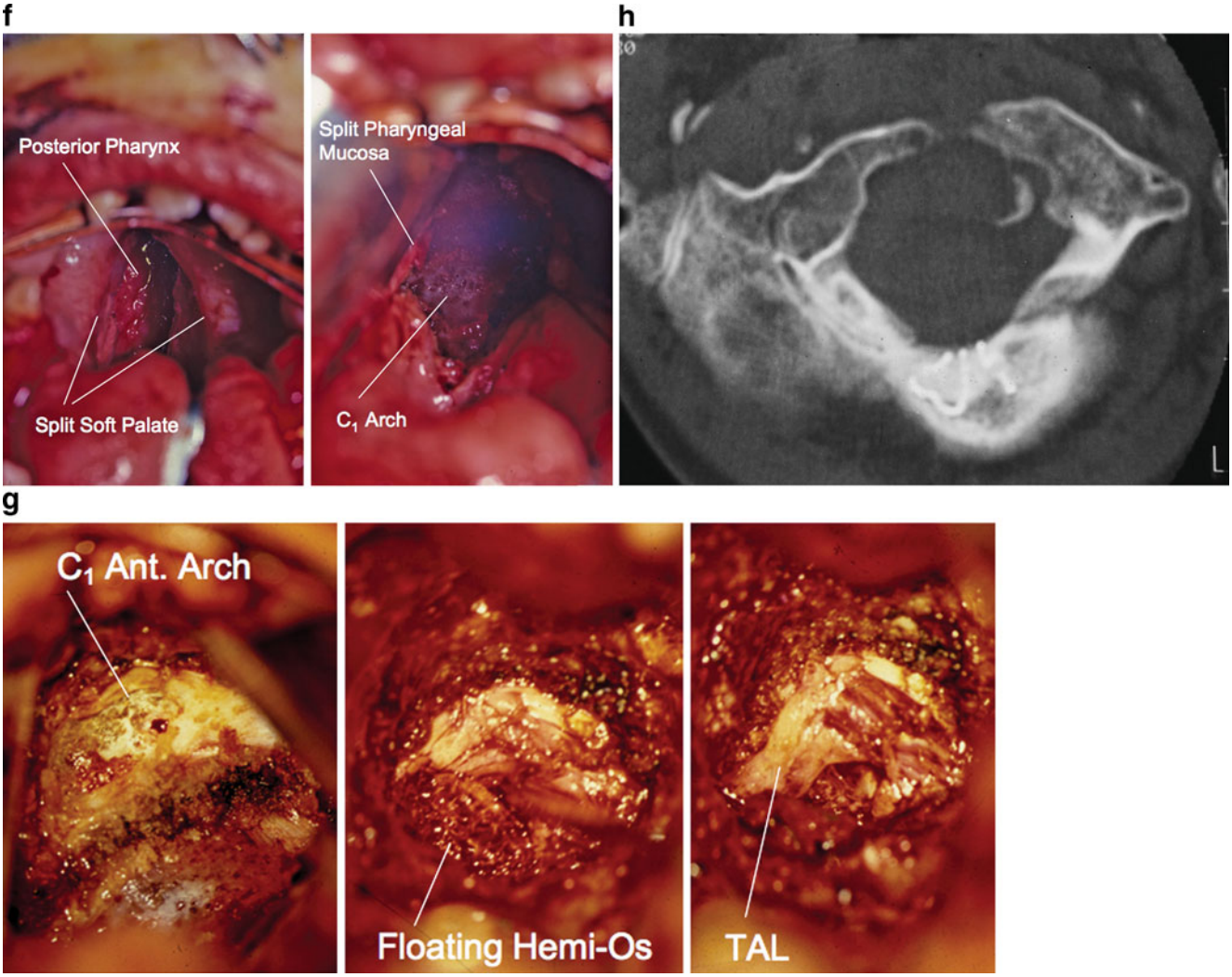

Fig. 34 (continued)

Hox code thus becomes translated into a specific vertebral anatomy [24, 33, 43].

The importance of the Hox code is illustrated by the severe abnormality in numbers and structures of vertebral segments when the code is altered by Hox gene mutations and teratogenic disturbance of Hox gene expressions. One example at the CVJ is the inactivation in mice of *Hox d-3*, an important component of the Hox code for the first cervical prevertebra. This results in a more caudal anterior boundary of *Hox d-3* expression, shifting the transitional sclerotomal properties from C_1 to C_2 prevertebra and transforming the C_1 prevertebra to a more anterior (i.e., occipital) identity, producing mutant mice with atlas assimilation to the basioccipital [13]. This is called anterior homeotic transformation (Fig. 21). Conversely, extension of an expression domain rostrally can transform prevertebral segments into a more caudal (posterior) identity, a phenomenon known as posterior homeotic transformation. This is exemplified in "gain-of-function" transgenic mutation of the murine *Hox d-4* gene, also a component of the Hox code for the C_1 prevertebra, such that its expression domain is forced to extend towards the occipital somites. The exoccipital region of the transgenic mutant shows no occipital condyles but instead ectopic neural arches resembling cervical neural arches, and the basioccipital is fused to the apical dens, "imitating" the behaviour of the atlas centrum [51] (Fig. 22). Thus, an altered interpretation of axial position cues in the developing occipital somites leads to an imposition of cervical vertebral phenotype upon the occipital bones. These observations suggest that Hox gene abnormality may underlie many malformations in the CVJ [17].

Pax-1: the resegmentation gene

The Pax family of regulatory genes is implicated in sclerotomal resegmentation. Pax genes in vertebrates all contain the highly conserved DNA sequence called "paired-box". There are nine *Pax* genes; all except *Pax-1* and *-9* are

involved in development of the central neuraxis. These two exceptions, especially *Pax-1* (*PAX-1* in the human homologue) [83, 97], control boundary formation between tissues by keeping two cell populations separate, presumably because the transcription factor encoded by *Pax-1* differentially regulates cell surface molecules expressed by these two cell populations, thereby divergently influencing their respective fates. This scenario of cellular partitioning is a necessary condition for resegmentation, and *Pax-1* action at the future IBZ thus helps to demarcate the site and extent of sclerotomal segregation. The downstream target gene for *Pax-1* is unknown, but may involve cell adhesion molecules such as NCAM or cytotactin, or molecules that promote cell-cell communication such as connexins [40, 41, 66, 83].

Pax-1 expression is detected very early in the pre-differentiated somites. Signals from the notochord and ventral floor plate of the neural tube, mediated by the SHH protein, induce the somite to divide into dermomyotome and the ventromedial sclerotome. This coincides with intense expression of *Pax-1* ventrally within the sclerotomal field, suggesting that *Pax-1* also plays a mediating role in the dorsoventral specification of somites [47, 99].

After somitic differentiation, *Pax-1* expression is noted within both the lateral and axial sclerotomes where its timing and fluctuating levels coincide with crucial events of resegmentation. For example, during condensation of the axial sclerotome into the loose and dense halves, *Pax-1* expression is weak within the loosely cellular prevertebrae but intense within the dense IBZ [83, 99]. Later, with chondrification of the prevertebra to form the homogeneous vertebral body, *Pax-1* is further actively repressed in this location, but persists in high levels at the IBZ where partition of centra takes place, until formation of the intervertebral disc is well underway [99]. *Pax-1* level is also enhanced during condensation of the lateral sclerotome to form the neural arch [23, 25, 98].

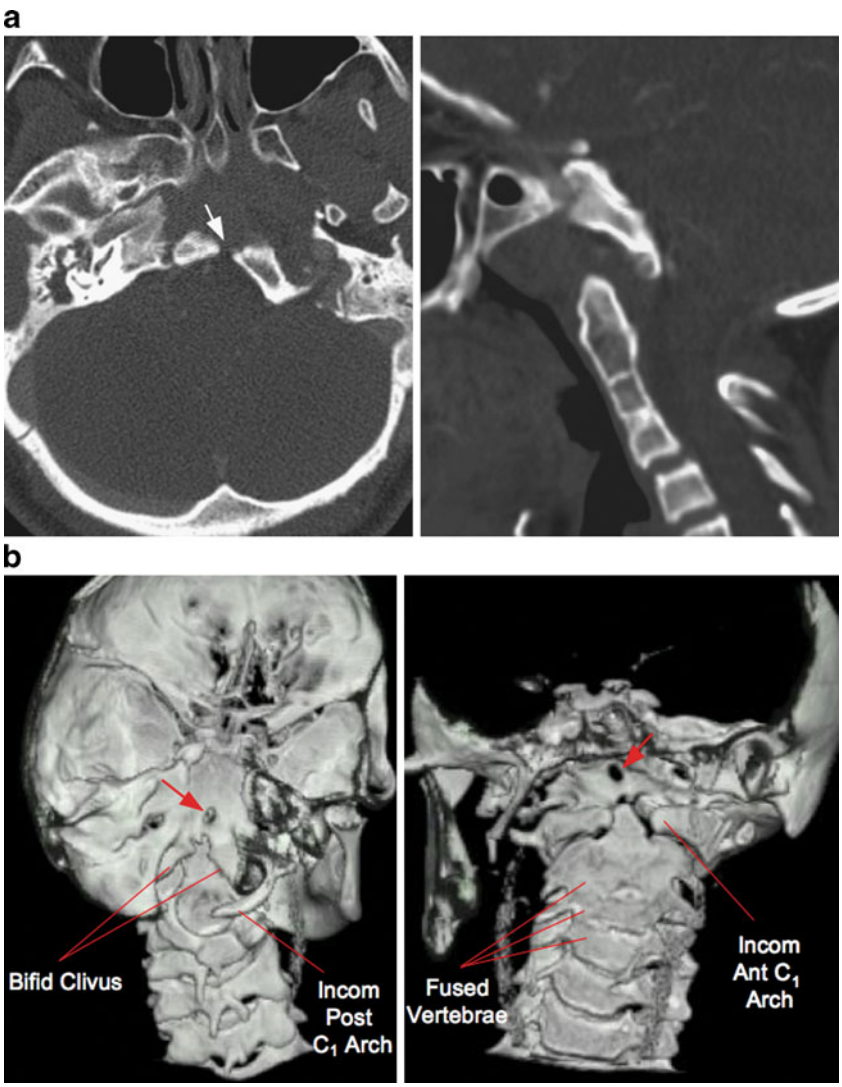

Fig. 35 Bifid clivus. **a** *Left*: Axial CT shows the gap in the lower clivus (*arrow*). *Right*: Sagittal CT shows the odontoid process is far anterior to its usual position below the clivus. Fusion of the C_2, C_3 and C_4 centra is also seen. **b** CT 3-D rendering of the skull base. *Left*: View from the back shows widely bifid basiocciput and an oval defect (*arrow*) higher in the clivus. The posterior C_1 arch is deficient. *Right*: view from the front shows the odontoid is far forward from the bifid clivus (mostly covered by the dens), and the anterior C_1 arch is also bifid. Note upper clival defect (*arrow*). *Incom post C_1 arch* incomplete posterior C_1 arch; *Incom ant C_1 arch* incomplete anterior C_1 arch

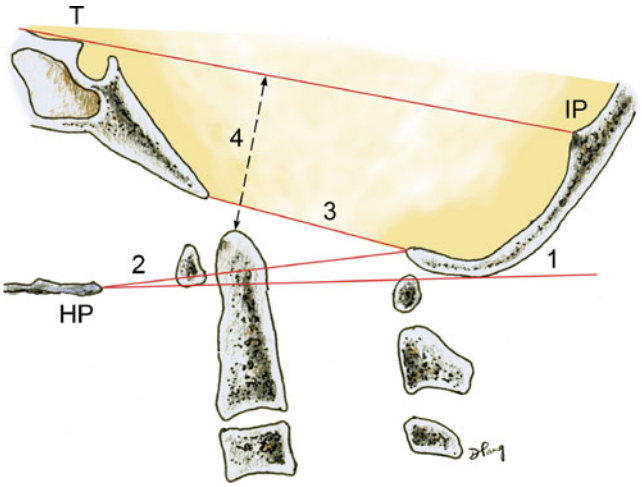

Fig. 36 Radiographic criteria for basilar impression. *1* McGregor's *line* between hard palate (*HP*) and the lowest point of occiput. Basilar impression is present if the dens protrudes >5 mm above this line. *2* Chamberlain's line between hard palate and opisthion. Positive diagnosis if dens protrudes >2.5 mm above *line*. *3* McRae's *line* between basion and opisthion should be above the dens. *4* Klaus index, distance between tip of dens and the tuberculum–cruciate line between tuberculum (*T*) and internal occipital protuberance (*IP*). This measures depth of the posterior fossa

Conversely, normal fusion of certain adjacent sclerotomes takes place only when *Pax-1* expression is turned off. At the CVJ of chick embryos, *Pax-1* repression is timed exactly when the occipital sclerotomes fuse to form the basioccipital. The fusion of the two dens primordia with the axis body also coincides with the down-regulation of the Pax-1 gene [99]. Ectopic *Pax-1* expression disrupts normal assemblage of the dens axis and basioccipital [98]. *Pax-1* is also highly expressed within the transitional zone between the proatlas and the first cervical sclerotome; it may thus also play a role in the separation of the head from the trunk.

Murine *Pax-1* mutants *undulated* show multiple fusion of vertebral bodies and fusion of the dens with the anterior atlantal arch [98], reminiscent of the human Klippel–Feil syndrome [84]. It is therefore conceivable that hyper- and hyposegmentation defects in humans may be explained by over- and under-expression of *PAX-1* during vertebral development.

Disturbance of the axial component of occipital sclerotomes, proatlas and C_1–C_2 sclerotomes: anomalies of the central pillar

There are two classes of central pivot anomalies: one concerns the dens–axis complex itself and includes the various forms of odontoid dysgenesis; the other afflicts primarily the basiocciput leading to an abnormal relationship between the odontoid and the skull base, comprising such entities as bifid clivus, platybasia, basilar kyphosis, basilar impression and a retroflexed dens.

Odontoid dysgeneses

The making of any part of the vertebral column requires the successful completion of three developmental phases: First, the mesodermal primordium has to be properly formed and, in some cases, assembled during the membranous phase; second, the mesodermal primordium undergoes chondrification in the cartilaginous phase; and finally, in the osseous phase, ossification takes place within the cartilaginous mold to complete the end product. In the case of the dens–axis, there is a fourth phase which involves bony fusion of the upper and lower dental synchondroses (Fig. 16).

The various forms of odontoid dysplasia are classifiable according to their probable pathogeneses, which, in turn, are traceable to failure of one or more of the four

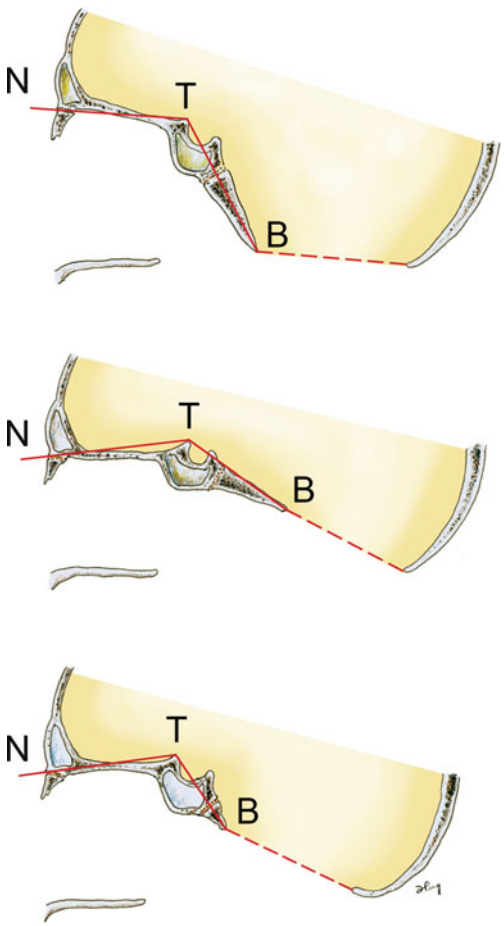

Fig. 37 Normal clival angle (*top*) measured by the NTB angle of Welcker joining the nasion (*N*), tuberculum (*T*) and basion (*B*). The angle should be less than 130°. Platybasia (*middle*) is marked by an increased NTB angle. This raises the basion and forces the foramen magnum plane (*dotted line*) to tilt upwards. The same upward tilt of this plane also occurs with a short clivus (*lower*)

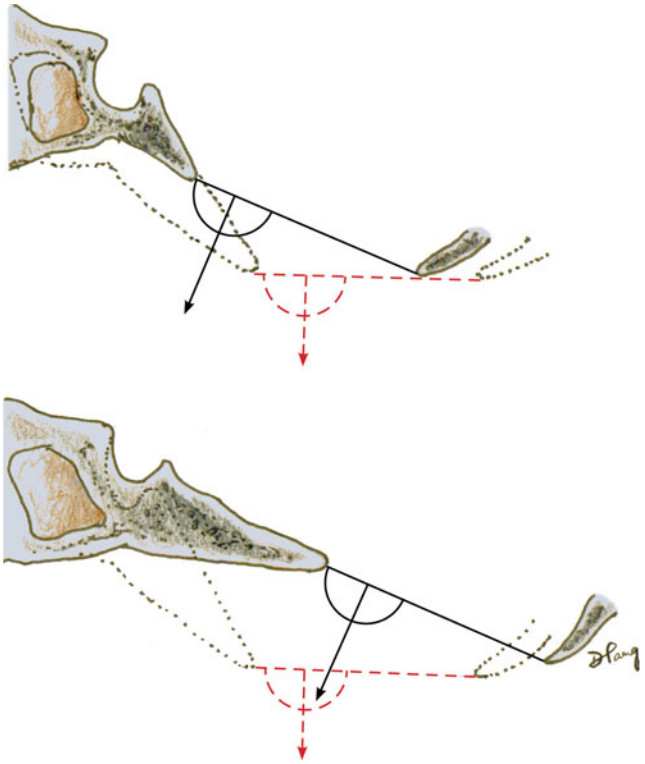

Fig. 38 Severe lordotic tilting of the plane of the occipital condyle in short clivus (*upper*) and platybasia (*lower*). Normal clivus and opisthion are represented by *dotted outlines*, and orientation and plane of the occipital condyle are represented by *arrow* and *semi-circle*, respectively; *red* for normal and *black* for abnormal

developmental phases. As with other types of bony malformations of the CVJ, four main developmental errors are encountered in odontoid anomalies:

1. Hyperplasia of primordium
2. Aplasia/hypoplasia of primordium
3. Disturbance of resegmentation
4. Failure of midline integration of primordium

Aplasia/hypoplasia of the axial sclerotome of proatlas and first cervical sclerotome: agenesis and hypogenesis of odontoid components

The odontoid process, or dens, develops from the axial sclerotome of the proatlas and first cervical sclerotome. Primordia of the apical and basal dental segments fuse with each other and to the C_2 centrum. Complete agenesis of both dental components is rare and usually occurs in the context of collagenopathy syndromes such as spondyloepiphyseal and spondylometaphyseal dysplasias (Fig. 23). Agenesis or hypogenesis of just the basal segment results in a stumpy dental pivot with a floating apical ossicle (Fig. 24). Both types are associated with instability. Agenesis of the apical segment is the most common variety by comparison. Radiographically, the dens is short although there is usually adequate pivot height for the transverse atlantal ligament and there is thus no instability (Fig. 25).

Complete odontoid agenesis in patients with collagenopathy or mucopolysaccharidosis such as Morquio's disease may not always be due to primordial failure since a completed cartilaginous mold of the dens has been seen in situ, where ossification was found to be defective because of the abnormal connective tissue production. Non-syndromic cases of odontoid agenesis, however, are usually due to aplasia or hypoplasia of centrum primordia. Treatment of symptomatic cases is usually C_1–C_2 fusion.

Disturbance of the intervertebral boundary mesenchyme of proatlas and first two cervical sclerotomes: os odontoideum and ossiculum terminale persistens

Aetiology Abrogation of the IBZ during early resegmentation such as in the transgenic mutant mice *undulated* causes exuberant fusion between sclerotomal units rather than lack of fusion [83, 99]. Thus, when there is non-fusion of

Fig. 39 Anterior form of basilar impression caused by an exceedingly short (<1 cm) and blunted clivus (*arrow*) with severe lordotic tilt of the plane of the foramen magnum, leading to a "sympathetic" lordotic bend of the dental pivot resulting in a retroflexed odontoid and basilar impression

discrete individual dental components as in os odontoideum and ossiculum terminale persistens, one may safely assume that the respective IBZ between the proatlas and the first two cervical sclerotomes were initially demarcated but subsequent development of the upper and lower dental synchondroses was unconsummated.

Os odontoideum There are endless debates in the literature about whether os odontoideum is truly a developmental anomaly or an un-united odontoid fracture. Proponents for the traumatic theory argue that the inferior surfaces of most os odontoideum are above the "expected base" of the normal dens, which is supposed to be below the level of the C_2 lateral masses [15, 17, 34–36, 58, 61, 94], and that there is often a "cupola" bulging cranially from the axis stump that represents the bottom half of a fractured dens [94]. In countering, the developmentalists point out that transgenic mutant experiments repeatedly show that vertebral primordia that have undergone aberrant development seldom evolve into the orthodox configuration of the normal phenotype, but instead become oddly shaped due to over-, under- or even erratic growth depending on the activities of local inducers [75, 83, 99]. The often expanded roundness of the os odontoideum with its corrugated horn-like corners (Fig. 26a) can hardly be the expected visage of an unhealed odontoid fracture, with its compromised blood supply. In addition, os odontoideum has been found in identical twins [46] and families [62], as well as amongst children with collagenopathies, and it frequently co-exists with other developmental bony anomalies of the skull base, all reinforcing the congenital theory. We believe that what has been called os odontoideum is a heterogeneous designation of both the congenital and post-traumatic varieties, but there may also be cases with mixed aetiologies. For example, the mesenchyme at the IBZ may have failed to chondrify and therefore cannot ultimately undergo ossification and fusion. As the two dental components ossify on opposite sides of the IBZ and gain mechanical leverage, the persisting mesenchymal tissue could no longer withstand the stress caused by foetal movements, and the upper part separates as the loose os odontoideum. The evidence for either theory is selectively circumstantial although the clinical implications are the same.

Ossiculum terminale persistens There is little dispute about the developmental origin of ossiculum terminale persistens. The ossiculum represents an unfused and detached apical dental segment, which comes from the proatlas centrum [18, 19, 36, 94] (Fig. 27). The detachment is probably due to upper dental synchondrosis failure although late disturbance of the third wave of odontoid ossification may be responsible. The ossiculum is usually non-syndromic although cases are seen with Morquio's disease.

Clinical significance Because the TAL straps around the basal segment of the dens, os odontoideum is at least potentially unstable (Fig. 28). Symptoms vary from persistent neck pain, torticollis, transient quadriparesis, lower cranial neuropathies, to recurrent brain stem strokes caused by stretching of the vertebral arteries and basilar artery embolism (Fig. 26b).

Although most ossiculum terminales are stable anomalies [17, 94] because the TAL's anchorage is not affected, we have encountered cases in which the basal dental segment is hypoplastic and the dental pivot is short. Some of these are conducive to atlantoaxial subluxation and high cord compression (Fig. 29a, b). Posterior C_1–C_2 fusion is adequate treatment if complete reduction is achievable. If there is persistent anterior dislocation of C_1, its posterior arch may have to be removed for decompression, in which case occipital C_2–C_3 fusion is necessary (Fig. 29c).

Illustrative case 1 A 10-year-old girl presented with intermittent quadriparesis and neck pain. Dynamic sagittal CT reconstruction shows an ossiculum terminale with anterior subluxation and only partial reduction on extension and persistent cord compression by the posterior arch of C_1 (Fig. 30a). The nearly spherical ossiculum forms a synovial joint with the posterior aspect of the anterior C_1 arch, and the two structures move together (Fig. 30a). Sagittal MRI shows an extremely narrow spinal canal at C_1 (Fig. 30b). C_1 laminectomy and instrumentation fusion of occiput to C_2–C_3 was performed. Her occiput had a robust midline keel so that a regular cruciate occipital plate was secured to the skull with three 6-mm screws (Fig. 30c) and then to two upright rods contoured to the region. The rods were affixed by interlocking links to bilateral C_1–C_2 transarticular screws and C_3 lateral mass screws (Fig. 30d).

Abnormal resegmentation of proatlas centrum—os avis

In this rare anomaly, the apical dental segment is attached to the basioccipital and is not fused to the main dental stem. The pivot is thus shortened but firmly fixed to the axis centrum, where a semi-lucent line representing the lower synchondrosis marks the successful integration of the two lower dens–axis components. This anomaly has been called "dystopic os odontoideum" by von Torklus and Prescher [75, 76, 94] to distinguish it from the "orthotopic os odontoideum" used by these authors to designate the common variety of os odontoideum. Their use of the term os odontoideum differs from ours in that they have included both the unfused basal and apical dental segments.

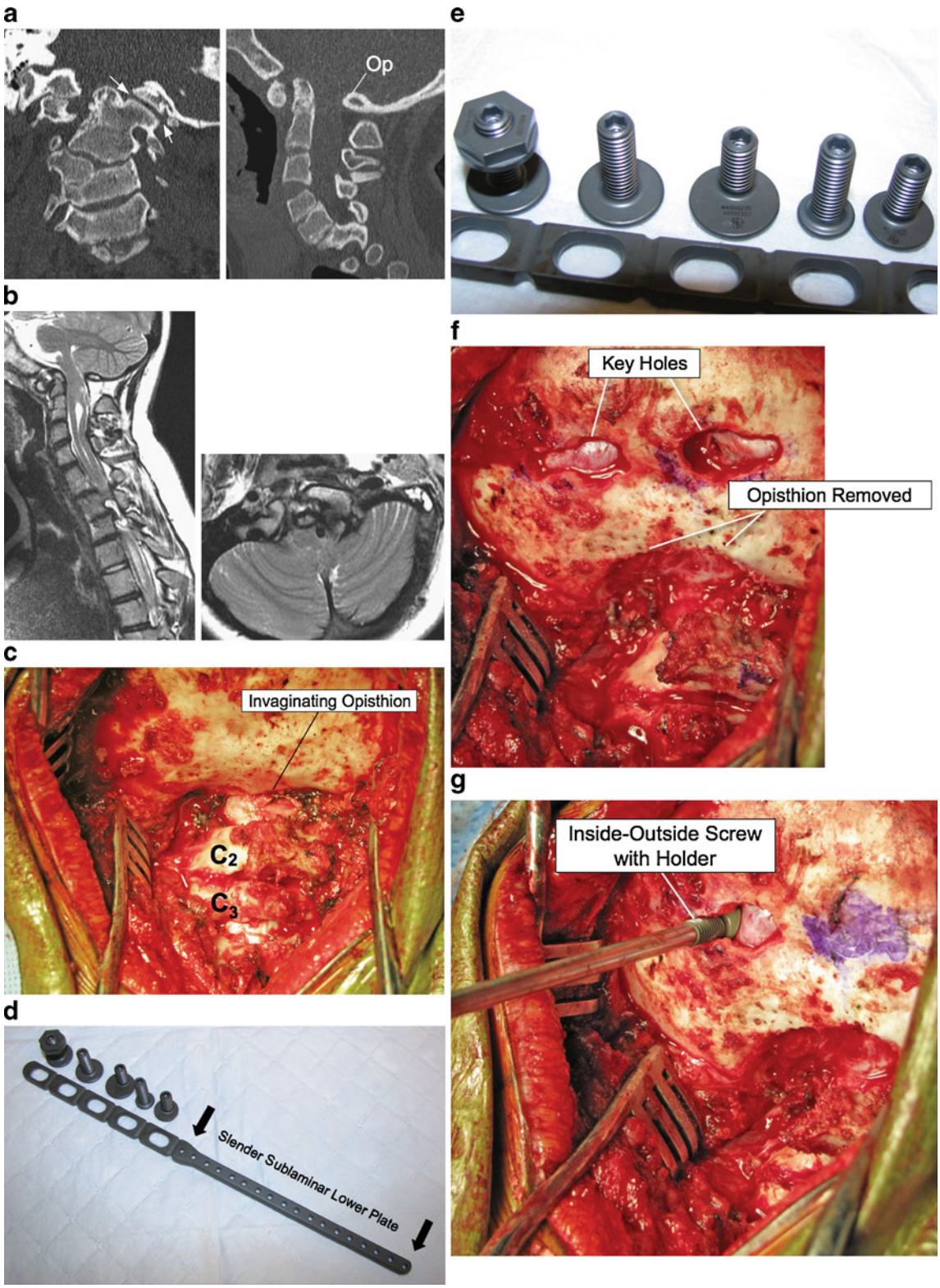

Embryogenesis In human malformations, it is not uncommon to find errant ontogeny reverting to a morphological pattern reminiscent of an organ's phylogenetic past. As case in point, a separate bone between the dens and the basioccipital resembling the attached ossiculum in the human anomaly is found in some fish and reptiles and many birds [29, 31, 39, 75, 76, 85, 100]; hence, our terminology os avis. In higher vertebrates, this bone, the

◀ **Fig. 40** Illustrative case 3 of the posterior form of basilar impression. A 12-year-old girl with occipital headache, neurogenic dysphagia and right hemiparesis. **a** CT of CVJ. *Left*: coronal CT shows severely upslanting and elevated left occipital condyle–C_1 joint (*arrows*). C_4 is a hemi-vertebra. *Right*: sagittal CT shows invagination of the opisthion (*Op*) (basilar invagination). The posterior arch of C_1 is assimilated into the posterior rim of the foramen magnum. Note slightly high-riding odontoid but absence of platybasia, short clivus or retroflexed dens. **b** Sagittal and axial MRI shows compression of the medulla by the invaginating opisthion and syringomyelia. **c** Intraoperative picture showing the invaginating opisthion and the rotated and knobbly spinous processes of C_2 and C_3. **d** The inside–outside screw plate with a slender sublaminar lower plate designed for sublaminar cable application for very young children. **e** Different inside–outside screws with different plate diameters (8–12 mm), screw-stem lengths (10–14 mm) and centre or off-set stems. The nut is shown with one of the screws. **f** Key holes in the occipital bone cut for insertion of the inside–outside screw. Note the invaginating opisthion lip has been removed. **g** Insertion of the inside–outside screw in holder. **h** Inside–outside screw (I–O screw) and plates in place with sublaminar cable round the laminae of C_2 and C_3. **i** Onlaid cortical and cancellous bone grafts (*G*) in place. **j** 3-D rendition of the fusion site at CVJ with the inside–outside screw (I–O screw) plates (I–O plate). *Right picture* and *inset* show subtracted CT 3-D images of the screw plates and sublaminar cables. **k** Post-operative CT. *Left* shows removal of the invaginating opisthion (*arrow*) and onlaid bone grafts (*G*). *Right upper* shows the inside–outside screw plate assembly with the flat screw head pointing inwards and the screw stem (I–O S) outwards. *Right lower* shows axial CT of the decompressed foramen magnum

primordium of the apical dens, normally becomes detached from the basioccipital rim, which shares with it a common origin in the proatlas centrum. Lack of proper resegmentation of the proatlas centrum, in essence negating the necessary cleavage, prevents descent and subsequent joining of the apical segment with the centrum of the first cervical sclerotome to complete the dental pivot. The reason for this failure is unknown, but since proatlas resegmentation normally occurs at the transitional zone between somites 4 and 5, a caudal shift of this transitional zone along the body axis may affect the resegmentation process. In transgenic mouse mutant in which *Hox a-7* is expressed earlier and more rostrally in its anterior domain, the last occipital somite (O_4) is transformed (posteriorly) to become the atlas, bearing a "proatlas" centrum that remains attached to the basioccipital. C_1 then becomes C_2 and acquires a complete centrum whilst C_2 is deleted of its normal dens [24]. This extra "proatlas" bone in the murine mutant very much resembles the os avis in the human malformation and suggests that a Hox gene mutation causing posterior homeotic transformation of segmental identity may indeed underlie the genesis of the os avis.

Clinical significance An os avis tends to be associated with neurological deterioration. The two patients with os avis described by Wollin [100] amongst seven others with "loose" ossiculum terminale and os odontoideum are the only ones with symptoms, and both had a hypoplastic dental pivot. Both cases of os avis described by Menezes and Fenoy are symptomatic due to posterior dislocations of C_1 on C_2 [60]. Of the two cases in our series, one had a hypoplastic dens and the atlantoaxial complex is extremely unstable on extension; the TAL is strapped against the os and therefore moves with the skull (Fig. 31). Our other case is associated with other CVJ anomalies such as multiple hyposegmentation of vertebral bodies, short clivus, basilar impression and a stenotic foramen magnum, even though the dens pivot is tall and sustaining for the TAL. The patient does not have instability but develops compressive symptoms (Fig. 32). In Wollin's cases, associated anomalies include a large median (third) occipital condyle (see below) and a hyperplastic anterior C_1 arch.

Treatment of os avis depends on the other anomalies. Pure instability can be remedied with C_1–C_2 fusion. An absent posterior C_1 arch or an occipitalized atlas would mandate inclusion of the occiput into the fusion. Concomitant neural compression due to basilar impression or invagination of the opisthion may require simultaneous decompression.

Failure of midline integration of basal dental segment: the bifid dens

Aetiology A completely bifid dens is an extremely rare entity. It is different from the "dens bicornis" described by von Torklus and Gehle in which only the tip of the dens is bicornuate and the function of the otherwise well-formed dental pivot is unaffected [94]. Dens bicornis results from aberrant distal ossification late in development. In true dental bifidity, the partition in the basal dental segment goes full length of the process to the lower synchondrosis. In one example, the bifid dens is accompanied by a dislocated ossiculum terminale (Fig. 33). In two others, one half of the split dental base is unattached to the centrum of C_2 and is floating free, whilst the body of C_2 is fused with that of C_3, which is itself bifid. The anterior C_1 arch is also unfused in the midline (see "Illustrative case 2"). These examples suggest that the lack of midline integration occurs very early in development, probably in the mesenchymal prevertebral stage or during chondrification. The lack of midline integration in the primordium of the basal dental segment appears to interfere with fusion of the adjacent synchondrosis leading to a detached "hemi-os" in two and an ossiculum terminale in the other. Also, faulty midline integration in the second example given here is not confined to the basal dens but also extends to the primordium of the C_3 centrum and the hypochordal bow of the first cervical sclerotome, which forms the anterior C_1

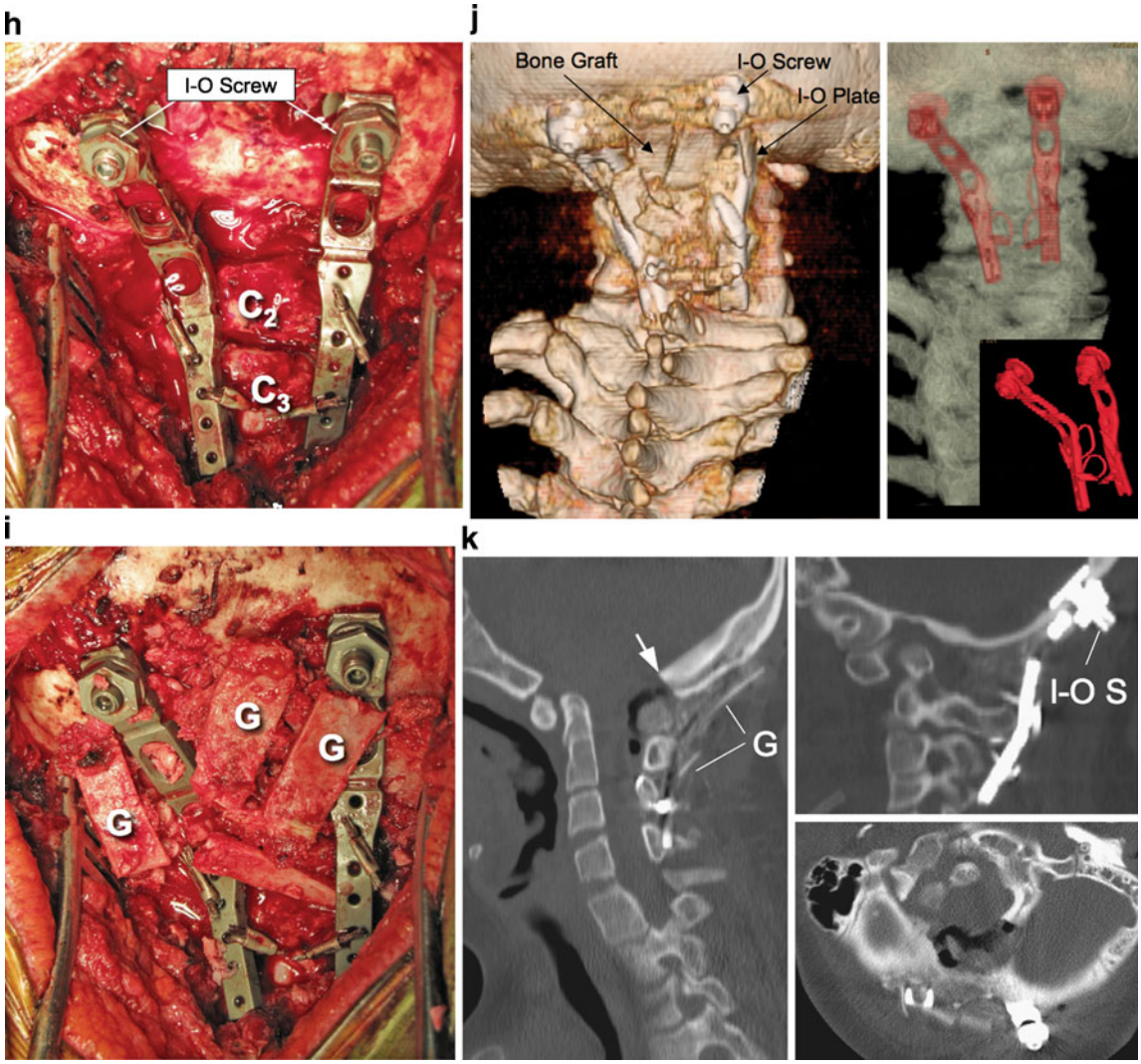

Fig. 40 (continued)

arch. The multiplicity of primordial abnormalities occurring around resegmentation would make it unlikely for a truly bifid dens to be a result of anomalous ossification, which occurs much later.

Clinical significance Our entire experience of three cases suggests that the bifid dens is associated with atlantoaxial instability because the central pivot is hypoplastic when bifid. In our first case, the hypoplastic dens is aggravated by the dislocated ossiculum terminale, negating any possibility for TAL anchorage (Fig. 33b, c). In our second and third case, the hypermobile "hemi-os" pops backwards during flexion and accentuates the cord compression (see "Illustrative case 2").

Stabilization for case 1 had to include the occiput into the fusion because of an incomplete posterior arch of C_1. In the other two cases, occipital–cervical fusion is combined with a transoral resection of both halves of the dens to relieve the anterior compression.

Illustrative case 2 A 6-year-old boy presented with intermittent quadriplegia and somnolence whenever he flexed his neck to study. CT showed a bifid odontoid with the right half unfused to the axis body (Fig. 34a) so that on flexion the mobile "hemi-os" popped backwards against the lower brainstem. A previous occipital–cervical fusion failed to relieve neural compression from the anterior vector (Fig. 34b). Because the boy also had congenital microstomia and micrognathia, which prevented a conventional transoral approach to the odontoid, we split the mandible, tongue, mylohyoid muscle and soft palate to access and resect the hemi-os and odontoid (Fig. 34c–g). The child recovered with complete abatement of symptoms (Fig. 34h).

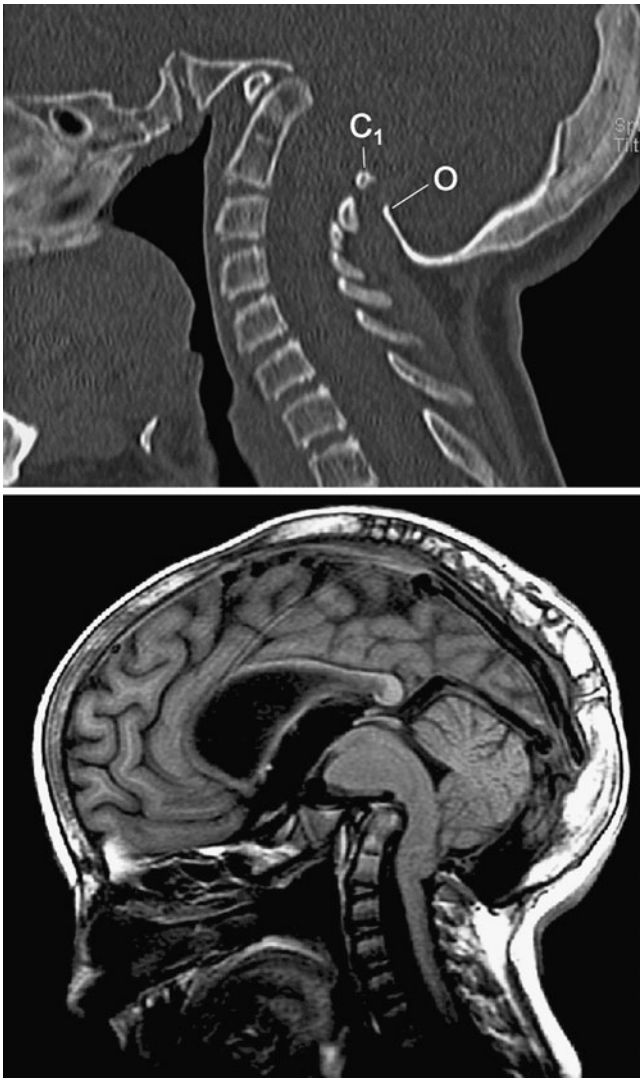

Fig. 41 Combined anterior–posterior form of basilar impression. **a** Sagittal CT shows extreme platybasia (NTB angle=180°), short clivus (<1.5 cm) and forward folding of the clivus–axis angle of Wackenheim (80°), causing lordotic tilt of the foramen magnum plane and plane of the occipital condyles, resulting in a retroflexed dens and severe basilar impression. Note violation of McGregor's, Chamberlain's and McRae's lines by the dens. Also, extreme invagination of the opisthion (*O*) and high posterior C_1 arch (C_1). **b** Sagittal MR shows distortion and compression of brainstem by both the dens and the opisthion

Basioccipital dysgeneses

Failure of midline integration of basioccipital primordium: bifid clivus

The rare entity of bifid clivus probably arises from failure of midline integration of the axial sclerotome of the proatlas, resulting in a split primordium of the basioccipital (Fig. 35). If the failure involves the other occipital sclerotomes, the bifidity may extend up to the sphenoclival synchrondrosis (Fig. 35a, right).

A widely split basioccipital may affect anchorage of the tectorial membrane, which normally straps the odontoid complex to the back of the clivus. The atlanto-occipital joint may become unstable and the cervical spine may appear to have drifted away from the skull (Fig. 35a (right), b). Treatment depends on the degree of instability and consists of occipito-cervical fusion.

Basilar impression, platybasia, retroflexed dens and basilar invagination

Basilar impression is suspected when the dens moves into the plane of the foramen magnum. It has been defined radiographically by the relationship of the tip of the dens with anatomical lines: McGregor's line, the most reliable, is

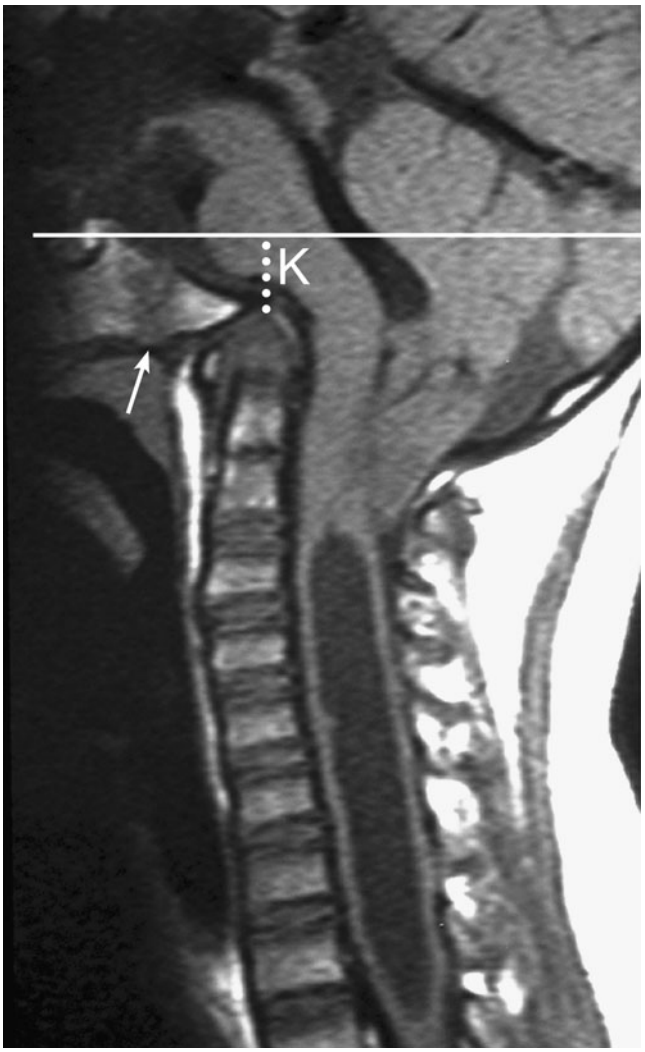

Fig. 42 Platybasia and short clivus (<1.5 cm; sphenoclival synchondrosis marked by *arrow*) causing severe basilar impression and mild retroflexed dens. This results in a shallow posterior fossa with a Klause index (*K*) of less than 1.8 cm and ectopic cerebellar tonsils and cervical syringomyelia

Fig. 43 Platybasia in a 9-year-old child with no symptoms. The clivus–axis angle (of Wackenheim) is about 100°. No CVJ compression is present

drawn between the hard palate and the lowest point of the occiput and should not be protruded by the dens for more than 5 mm. Likewise, Chamberlain's line between the hard palate and the opisthion should not be crossed by more than 2.5 mm, and McRae's line between the basion and opisthion not at all [55, 56] (Fig. 36). These lines were devised in the pre-MRI era. Today, the sagittal MRI is by far the best way to assess the clinical relevance of basilar impression.

Aetiology Congenital basilar impression, which concerns us here, is less a result of active upward indentation of the dens against the brainstem, as the word "impression" implies, than a drop of the posterior fossa contents on to the erect dens due to a shallow occipital "box" and flattened skull base. The causative occipital dysplasia is due to deformed growth of all three parts of the occipital primordium: the basioccipital (pars basilaris) and the exoccipital (pars lateralis including the condyles and the foramen magnum rim), which enlarge by endochondral ossification, are primarily hypoplastic; and the supraoccipital, the squama, which expands by membranous ossification and therefore depends on growth of the chondrocranial molds of the other two parts, is obligatorily constricted.

Three types of congenital basilar impression can be distinguished. Anterior basilar impression is caused by changes in the basioccipital complex, which derives from the axial (median) occipital sclerotomes. The most dramatic change is platybasia, when the nasion–tuberculum–basion angle (NTB angle of Welcker) is increased and the sphenoclival block appears severely flattened. Platybasia is often accompanied by a shortened basioccipital or clivus, which normally measures more than 3.2 cm from the spheno-occipital synchondrosis to the basion. The summated effect of a short and flattened clivus is that the basion, which normally lies below the nasion–opisthion line (of Boogaard), is raised way above it and moves cranially (Fig. 37). This forces the plane of the foramen magnum to tilt upwards in a lordotic angle and with it the planes of the occipital condyles and of the condyle–atlas articulations (Fig. 38).

The fusion and chondrification of the basioccipital and the exoccipital sclerotomes occur slightly earlier than the resegmentation of the C_1–C_2 sclerotomes. A severely lordotic skull base angle consequently forces the emerging upper cervical sclerotomal column to bend backwards "in sympathy", especially its centra complex that will ultimately form the dens–axis (Fig. 39). This explains why platybasia and short clivus are frequently associated with a retroflexed and lordotic dens, that, in severe cases, points sharply and wickedly backwards into the brainstem (Fig. 39). Clinical studies have indeed shown that patients with basilar impression have a significantly shorter clivus than control groups [67].

In the posterior form of basilar impression, the exoccipitals, derived from the lateral sclerotomes of the proatlas, rise up towards the foramen magnum, bringing with them the occipital condyles and opisthion. Alternatively, the exoccipital bones may be thin and the condyles flat and hypoplastic. In either case, the dens is secondarily elevated towards the cranial cavity without being lordotic or retroflexed. The opisthion, however, often invaginates into the cranial aperture (basilar invagination).

Illustrative case 3 A 12-year-old girl of normal intelligence presented with occipital headache, neurogenic dysphagia, nasal voice and right arm and hand clumsiness. CT showed a steeply elevated occipital condyle (exoccipital), basilar (opisthion) invagination and C_1 assimilation (Fig. 40a). There is no platybasia, and the dens, though migrated cranially into the foramen magnum, was not retroflexed (Fig. 39a, right). MR showed severe brainstem and upper cord compression mainly from the invaginating opisthion (Fig. 40b). At surgery, the posterior lip of the foramen was removed by careful drilling under microscopy (Fig. 40c). The thin occipital bone and the bizarre shapes of C_2 and C_3 precluded the use of regular occipital screw plates and intraaxial cervical screws. We used instead the inside–outside occipital screw plate system affixed to the C_2 and C_3 laminae with sublaminar cables (Fig. 40d–h). Onlaid autogenous iliac crest grafts were put in place (Fig. 40i–k).

In the combined anterior and posterior form, severe basilar impression by a retroflexed dens is accompanied by

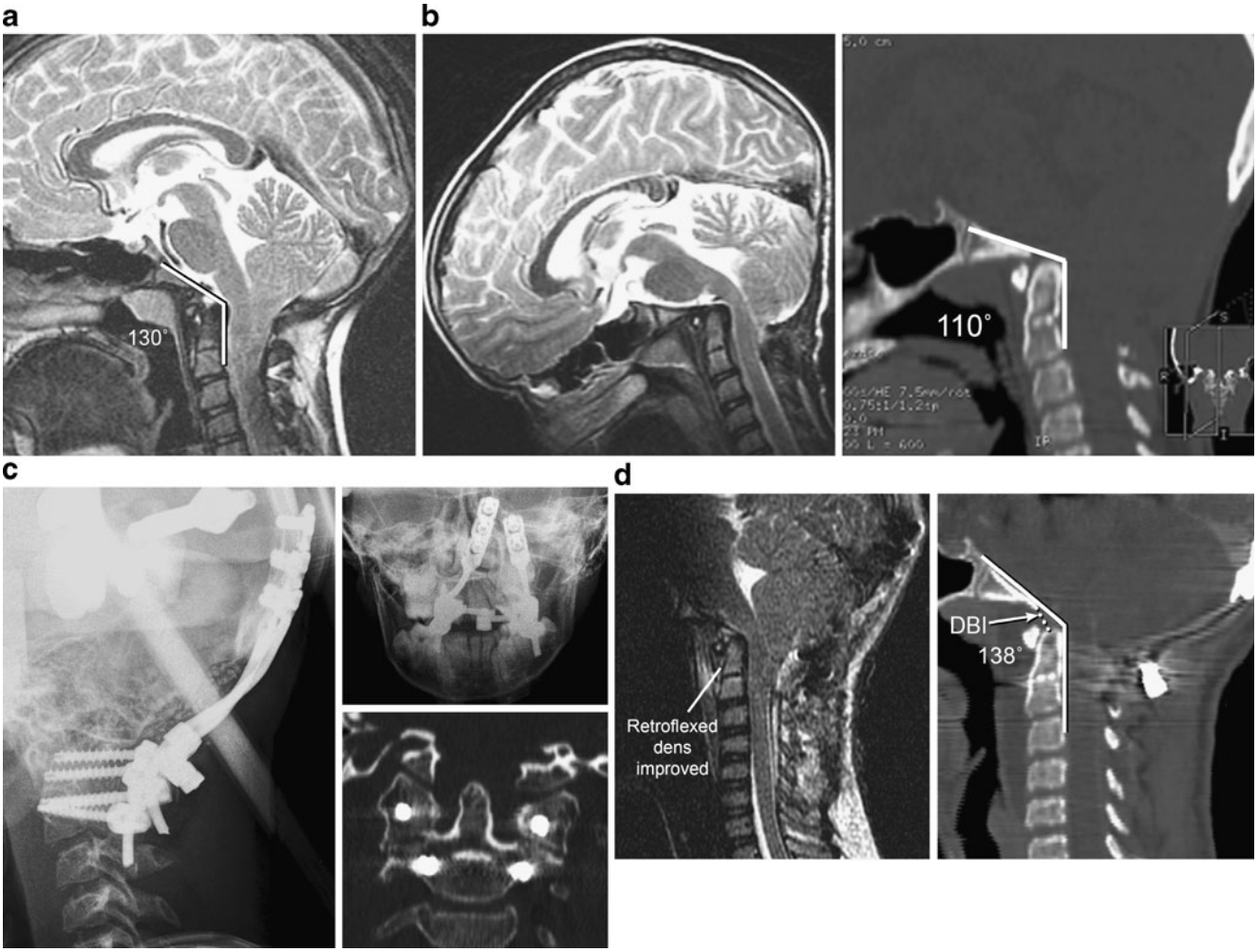

Fig. 44 A 12-year-old girl with retroflexed dens, mild basilar impression and Chiari I malformation. **a** Pre-operative clivus–axis angle (of Wackenheim) of 130°. **b** Post-operative cranial settling causing forward folding of Wackenheim's angle to 110° and shortening of dens–basion interval (*DBI*). Note worsened anterior brain stem compression. **c** Caliper traction (*left*) for 4 days followed by C_1–C_2 Goel-Harm's screw plate posterior fusion. **d** Post-fusion reversal of Wackenheim's angle to 138° and increase of DBI to 1.8 cm. Note relief of brainstem compression and symptoms

Fig. 45 Pre-basioccipital arch (*thin arrows*), a U-shaped bony valance on the ventral lip of the anterior foramen magnum rim. This results from complete preservation of the hypochordal bow of the proatlas

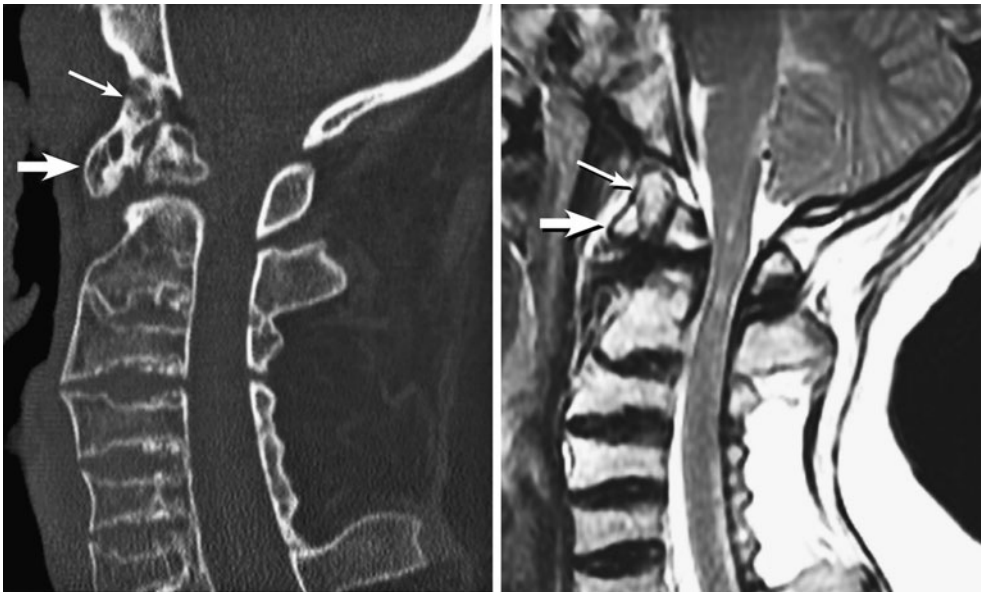

Fig. 46 Third occipital condyle or condylus tertius (*thin arrow*) attached to the ventral surface of the clival tip and fused to the anterior atlantal arch (*thick arrow*). On MRI, the condyle appears to form a synovial joint with an ossiculum terminale that is unfused to the basal dens. The third occipital condyle represents midline hyperplasia of the proatlas hypochordal bow

posterior invagination of the opisthion, causing neural compression from both front and back.

Illustrative case 4 A 12-year-old girl presented with occipital headache, hemi-sensory loss and tongue fasciculation. CT shows an essentially flat nasion–tuberculum–basion line and severe platybasia, an acute Wackenheim angle (basilar kyphosis), an elevated retroflexed dens and severe basilar (opisthion) invagination (Fig. 41).

The upward migration of the anterior and posterior occiput in severe basilar impression in essence reduces the posterior fossa volume, estimated by the index of Klaus, which measures the distance between the tip of the dens and the tuberculo-cruciate line (between the tuberculum sellae and the internal occipital protuberance) (Fig. 36). This index should exceed 30 mm [94]. With significant reduction to below 25 mm, the developing cerebellum and brainstem are desperately crowded and herniate downwards, accounting for the common association of ectopic cerebellar tonsils (Chiari I malformation) with severe basilar impression, platybasia, shortened clivus and retroflexed dens (Fig. 42). Occasionally, the lower brainstem also lies well below the plane of the foramen magnum ("Chiari 1.5") [89]. It is our impression that the truly congenital form of Chiari I malformation often includes skull base dysplasia, and the much debated acquired

Fig. 47 A short third occipital condyle (*arrow*) curving forward from the clival tip away from the foramen magnum

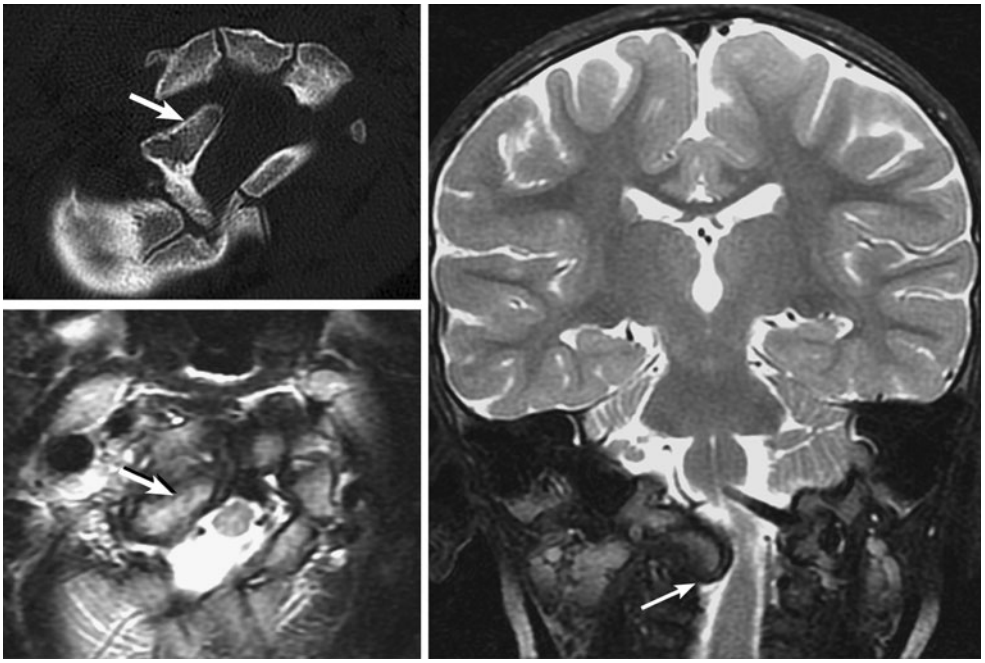

Fig. 48 Unilateral hyperplasia of the occipital condyle (*arrow*) with cervicomedullary distortion. This represents hyperplasia of the exoccipital (lateral) sclerotome of the proatlas

Chiari I malformation consists only of ectopic cerebellar tonsils. Studies have shown that patients with hindbrain herniation and basilar impression have a higher brain to posterior fossa volume ratio than those with just hindbrain herniation, and both groups have higher ratios than controls [67, 87, 90].

Clinical significance Platybasia without basilar impression is asymptomatic (Fig. 43). Indentation of the anterior medulla by the dens, however, produces brainstem dysfunction and lower cranial neuropathies more frequently than "pure" cerebellar ectopia without an anterior compression vector. The brainstem deficits include neurogenic dysphagia [70, 71], nasal or hoarse voice due to paresis of the palatal levator and vocal cords, sleep apnea and intermittent or progressive spastic quadriparesis. Tussive headaches, syncope and gait discoordination are also common complaints.

Posterior decompression for Chiari I malformation with coexisting basilar impression carries a much higher late complication rate than for pure cerebellar ectopia. Even if the anterior vector is not initially symptomatic, the slightest amount of post-operative cranial settling after nullification of the dorsal tension band will deliver the brainstem straight on to the pointing dens to cause rapid onset of new brainstem signs [32]. In addition, platybasia and a decrease

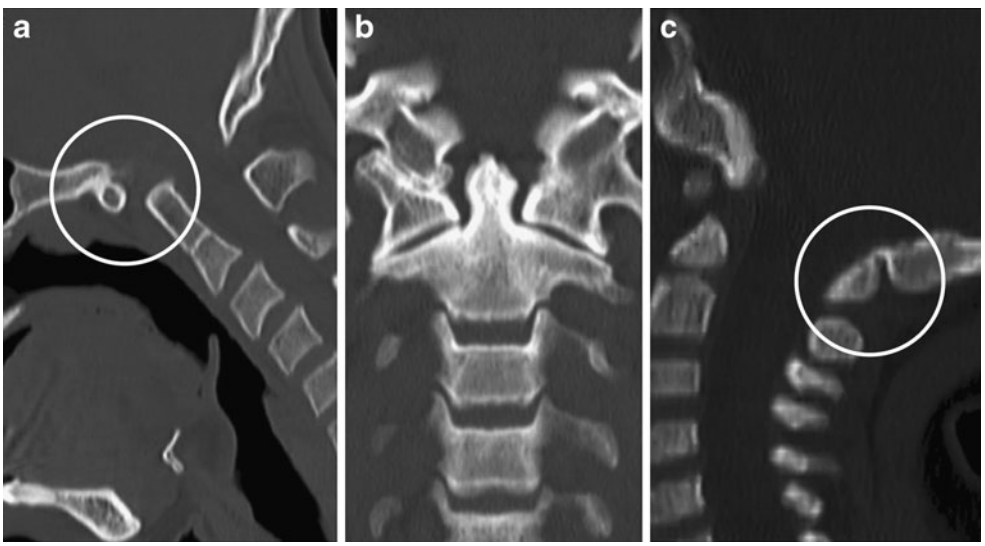

Fig. 49 C_1 assimilation or occipitalization. **a** Assimilation of the anterior atlantal arch (zone 1 assimilation). **b** Assimilation of the lateral masses (zone 2 assimilation). **c** Posterior arch (zone 3) assimilation

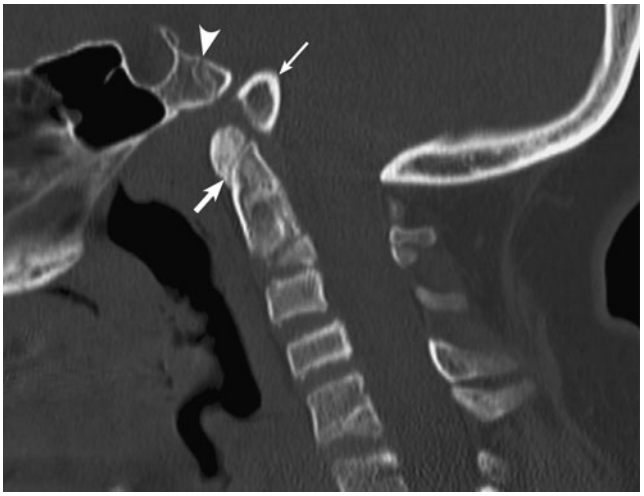

Fig. 50 Unfused clivus to basioccipital. The clivus or lower basioccipital segment (*thin arrow*) is unfused to the upper basioccipital segment, which is attached to the sphenoid bone at the spheno-occipital synchondrosis (*arrow head*). The anterior atlantal arch (*thick arrow*) is fused to the apical dens to form a "pseudo-centrum" for C_1. This may represent posterior homeotic transformation

in the clivus–axis angle (of Wackenheim) (basilar kyphosis) accentuate the forward bending moment acting on the clivus–dens pivot point and accelerate the forward "folding" of the cranio-cervical axis (see "Illustrative case 5" below). It is our distinct impression that this type of post-operative instability occurs far more commonly in the associative type of Chiari I malformation. We therefore avoid removing the C_2 lamina during the decompression, if necessary at the expense of resecting the tips of the tonsils.

If symptomatic post-decompression cranial settling does occur despite precautions, calipers skull traction with the neck in slight extension should be rendered under muscle relaxation and sedation for a few days, aiming at reversing the kyphotic deformity and telescoping effect at the foramen magnum. Occiput–C_1–C_2 fusion should be done after reduction. If brainstem indentation persists, transoral resection of the dens may be necessary.

Illustrative case 5 A 10-year-old girl presented with neck pain, diminished gag reflex, hand clumsiness and poor truncal coordination. MRI and CT showed cerebellar ectopia, basilar impression, a retroflexed dens and mild platybasia. The pre-operative clival–axis angle was 130° (Fig. 44a). The child improved after suboccipital craniectomy and C_1–C_2 laminectomy. Six weeks after surgery, the child presented with rapid onset of nasal food regurgitation, nasal voice, loss of gag reflex and aspiration. MRI and CT showed cranial settling, extreme basilar kyphosis with the Wackenheim angle now reduced to 110° and a shortened dens–basion interval (DBI) (Fig. 44b). Reduction with skull calipers traction and subsequent occipital C_1–C_2 fusion (Fig. 44c) promptly reversed her neurological defects. Post-fusion MRI and CT showed relief of the anterior basilar impression, straightening of Wackenheim's angle to 130° and restoration of the initial DBI (Fig. 44d).

Disturbances of the lateral sclerotomes and hypochordal bows of proatlas and C_1 sclerotome: anomalies of the surrounding ring structures

These can be divided into anomalies of the proatlas and of the C_1 resegmented sclerotome.

Anomalies of proatlas

Hyperplasia of the proatlas hypochordal bow—third occipital condyle

Embryogenesis The hypochordal bow is an arcual strip of mesenchyme ventral to the axial sclerotome. In humans, only the hypochordal bows of the proatlas and C_1 resegmented sclerotome persist [65]. The hypochordal bow of the proatlas normally forms a small midline osseus tubercle attached to the ventral surface of the basioccipital below the rim of the foramen magnum (Fig. 14). Rarely, it remains as a fully ossified structure distinct from the basioccipital bone. If the entire arc is preserved, it is called a pre-basioccipital arch, which looks like a U-shaped bony valance on the underside of the anterior rim of the foramen magnum [75, 92, 94] (Fig. 45). If only the paramedian arch persists, two parasagittal spikes project downwards from the clivus, called the basilar processes [75, 92, 94]. Neither of these bony excrescences encroach on the foramen magnum and are thus harmless. Occasionally, however, the median portion of the proatlas hypochordal bow becomes exuberantly hyperplastic and forms a prominent bone spur that juts obliquely backwards from the basioccipital tip, that does cause neural compression. This median bony process is firmly attached to the basion and, elongating it, frequently forms true synovial joints with the anterior arch of C_1 and the odontoid apex (Fig. 46) [92]; it is thus rather aptly termed a median or third occipital condyle (condylus tertius) [48] [74, 77, 92, 94]. These articulations, though bizarre, are not surprising if one remembers that the anterior arch of C_1 comes from the hypochordal bow of the first cervical sclerotome directly subjacent to the hypochordal bow of the proatlas, and the dental apex develops from the proatlas centrum; joint formation between corresponding components of adjacent sclerotomes is "normal" in the lower vertebral levels.

Clinical significance A third occipital condyle may be mistaken for an os avis on radiographs since both are osseous appendages of the clival tip. However, it is important to distinguish them because of their very different implications of stability. In os avis, the dental pivot has lost its top and becomes perilously hypoplastic, whereas the dental pivot in the case of the third occipital condyle has normal height and therefore remains solid anchor for the TAL; instability is unlikely. Although some third condyles are short and protrude along the contour of the clivus or even curl forward away from the brainstem (Fig. 47), others can be enormous backward pointing cantilevers [48, 60, 77, 94] producing serious neurological deficits. Because there is no instability, transoral, transclival resection of the third condyle is an adequate treatment.

Hyperplasia of exoccipital sclerotome—hypertrophic occipital condyle

Hyperplasia of the lateral sclerotome of the proatlas, precursor to the exoccipital bone, results in hypertrophy of the lateral and posterior rim of the foramen magnum including a massively gnarled occipital condyle. Bilateral condylar hypertrophy causes pincers-like cervicomedullary compression and early symptoms [60], but unilateral hypertrophy can also lead to severe lateral distortion of the lower brainstem and slow neurological deterioration. An uneven atlanto-occipital joint surface and chondromalacia may also produce chronic neck pain and stiffness. Treatment consists of resection of the occipital condyle, followed by occiput–cervical fusion for the expected O–C_1 instability.

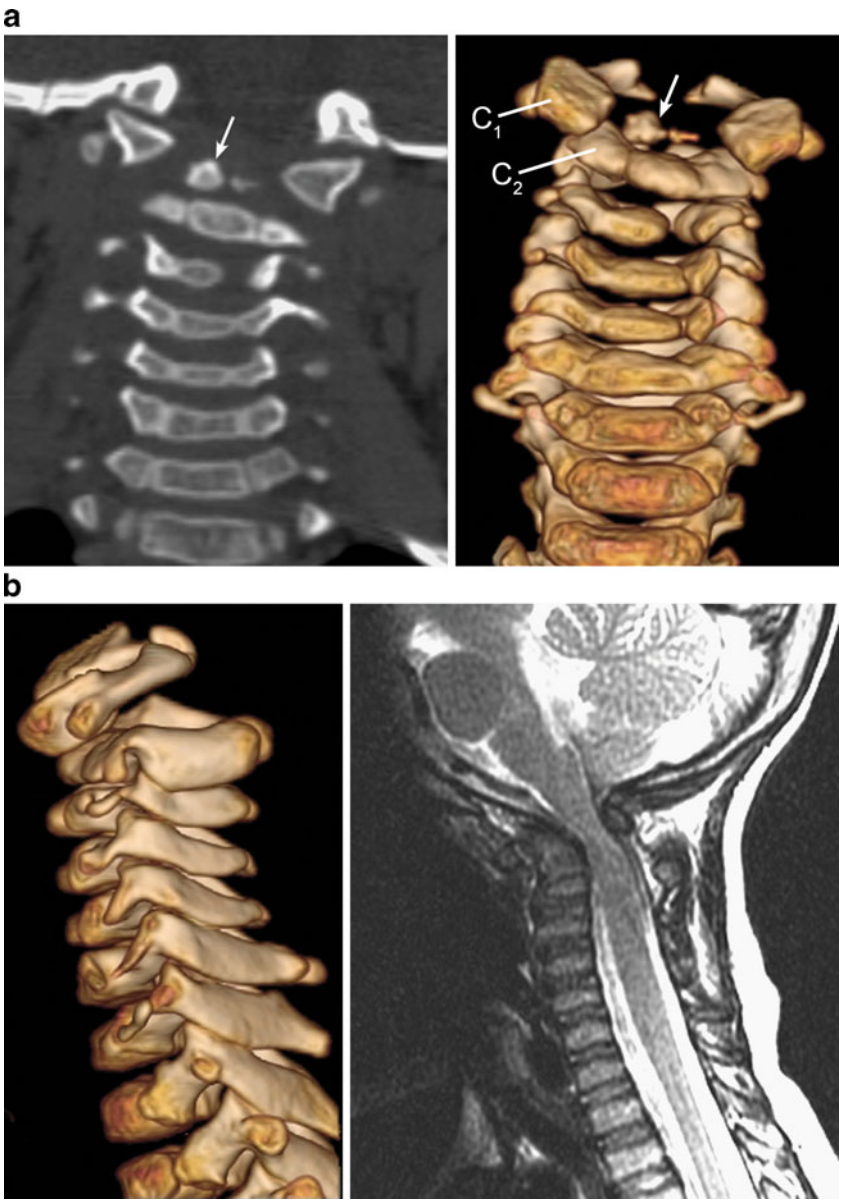

Fig. 51 Complete aplasia of C_1 hypochordal bow—complete aplasia of C_1 anterior arch. **a** CT and 3-D reconstruction shows no anterior atlantal arch or insertion tubercles for the TAL. The two anterior stunted dental hemi-os (*arrow*) are unfused to the C_2 centrum. Posterior arch of C_1 is also unfused. **b** Extreme C_1–C_2 flexion instability and severe cord compression

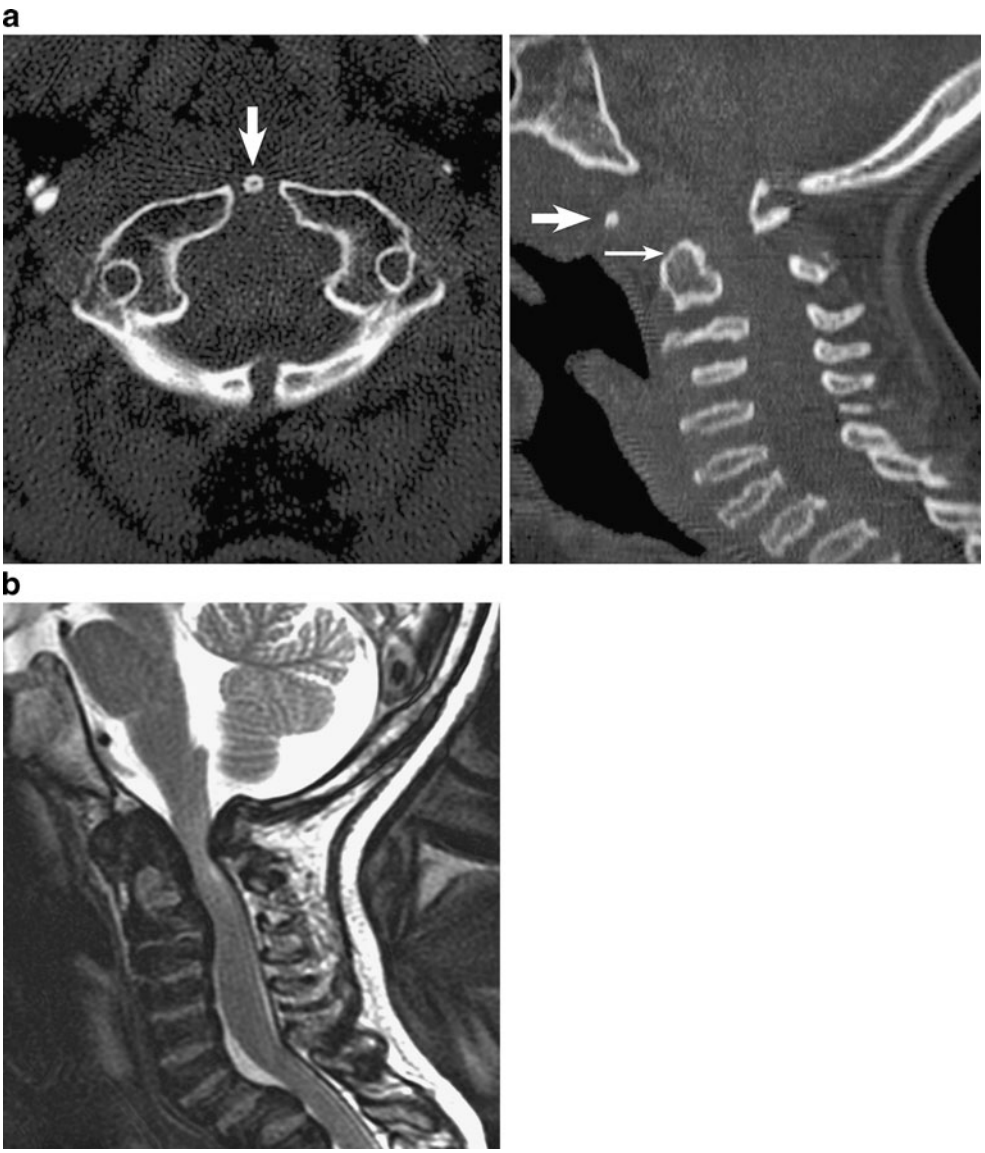

Fig. 52 Severe hypoplasia of C_1 hypochordal bow—small anterior C_1 arch. **a** Match-head size anterior C_1 arch (*thick arrow*) associated with complete agenesis of the dens (*thin arrow*), a result of concomitant C_1 centrum aplasia. **b** C_1–C_2 instability with cord compression

Illustrative case 6 A 6-year-old boy was born with a fixed torticollis. At age 5, he began complaining of worsening neck pain and loss of rotation. He presented after a gentle fall on his back with right arm and leg weakness. CT and MRI showed a severe lateral tilt of the craniocervical junction, gnarly hypertrophy of the right occipital condyle and compression and lateral distortion of the C_1 cord (Fig. 48). A right far lateral approach was used to resect the condyle–C_1 joint followed by occiput–C_1–C_2 fusion.

Assimilation of atlas—non-resegmentation of the proatlas sclerotome

Congenital fusion of the atlas with the occiput is one of the most common anomalies of the CVJ, with a prevalence rate from 0.08% to 2.8% in the general population [5, 8, 52, 88]. Atlantal assimilation, or occipitalization, ranges from complete incorporation of the atlas into the occiput to discrete osseous bridges between the two. Gholve et al. [30] identified three fusion zones. Zone 1 assimilation involves the anterior atlantal arch in front of the lateral masses (20% in their series); zone 2 assimilation involves primarily the lateral processes (17%); and zone 3 assimilation is fusion at the posterior atlantal arch (13%) (Fig. 49). Combination of zones is seen in over 50% of patients [30]. Thirty-seven percent of Gholve's patients also had associated basilar impression, 20% had Klippel–Feil syndrome, 17% Chiari I malformation and 37% had cervical stenosis.

Embryogenesis It has already been mentioned that inactivation of *Hox d-3* gene expression in mice results in anterior homeotic transformation at the CVJ such that the C_1 vertebra takes on an occipital identity and the head–neck

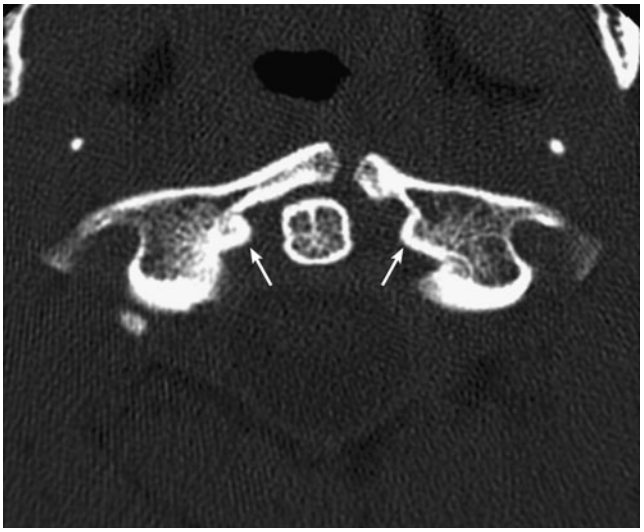

Fig. 53 Complete agenesis of posterior atlantal arch and bifid anterior atlantal arch. Normal TAL insertion tubercles (*arrows*). There is no C_1–C_2 instability

transitional zone moves caudally to the C_1–C_2 junction (Fig. 21). All mutants have assimilation of C_1 to the basiocciput [13, 24]. It is therefore tempting to ascribe human cases of isolated C_1 assimilation to similar mutations of the human *Hox* gene homologues. However, in cases of combined C_1 assimilation and Klippel–Feil syndrome in which multiple levels of cervical fusion are seen below C_2, the *Hox* gene theory will require multiple *Hox* mutations and alterations of multiple *Hox* codes, which is highly improbable. Since *Pax-1* expression is involved in resegmentation of all levels of the embryonic axis, inappropriate repression of *Pax-1* at the proatlas–C_1 sclerotome interphase and other vertebral levels may be involved in associative cases of atlas assimilation.

Clinical significance Assimilation of the atlas to the occiput means that the first mobile segment between the skull and spine has been transferred to the C_1–C_2 junction, as are all the motion stresses including that of flexion–

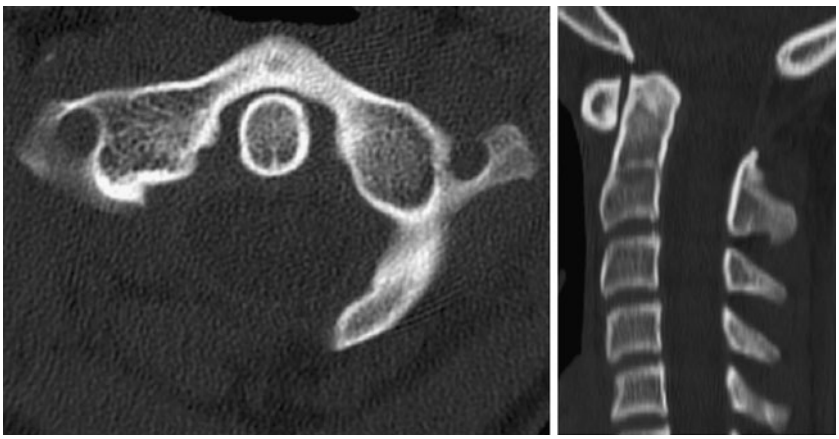

Fig. 54 Unilateral aplasia of the right posterior arch of C_1

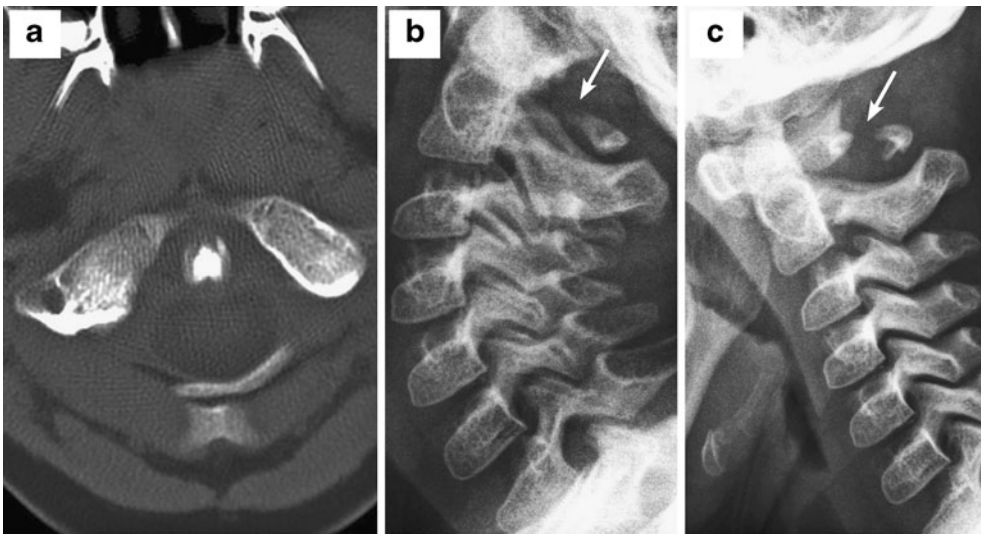

Fig. 55 Partial agenesis of posterior atlantal arch. **a** The posterior tubercle and arch remnant appear floating and unconnected to the lateral masses. **b**, **c** Flexion and extension shows ample tilting of the lateral masses away from the posterior tubercle (*arrows*), suggesting absence of a cartilaginous mold. In spite of this tilting, there is no translational instability

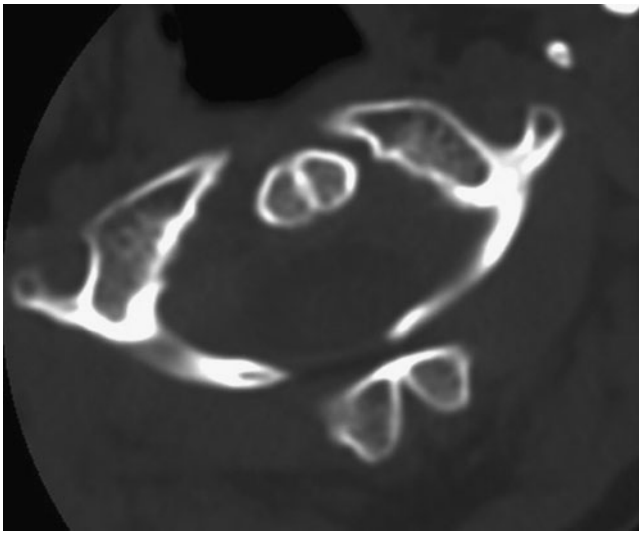

Fig. 56 Combined anterior and posterior atlantal arch defects

extension, normally of restricted range at this level and for which the local joint anatomy is ill suited. This also means the supporting myoligamentous structures are more likely to suffer "over-stretch" failure. Almost 60% of Gholve et al.'s patients with C_1 assimilation has C_1–C_2 instability defined as an atlantal–dens interval (ADI) greater than 4 mm in adults and 5 mm in children [30]. McRae and von Torklus and Gehle had similar findings [55–57, 93]. More than half of Gholve et al.'s patients with instability also had C_2–C_3 fusion, which adds to the burden of stresses at C_1–C_2.

The symptoms of C_1–C_2 instability range from persistent neck pain and stiffness to frank myelopathy. Typically, the neurological deficits begin in the third or fourth decade of life [55] and tend to worsen with age [56]. We have also seen concomitant hypertrophy of the posterior arch of C_2, which accentuates the neural compromise. Management for symp-

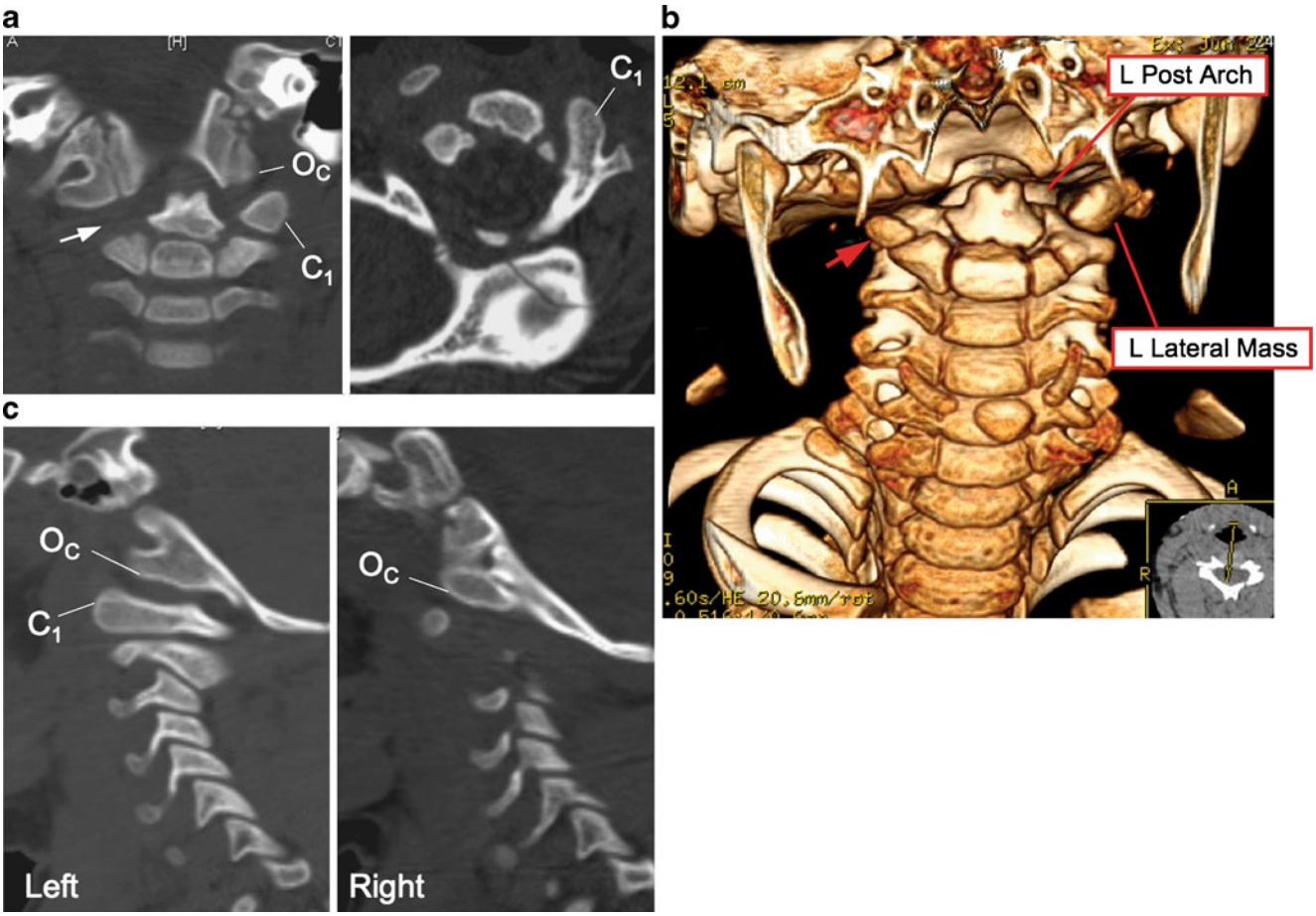

Fig. 57 Unilateral lateral mass aplasia in a 2-year-old with fixed right head tilt. **a** *Left*: Coronal CT shows aplasia of the right lateral mass. There is no real condyle–cervical articulation on the right side (*arrow*). Left Oc–C_1 joint is present. *Right*: aplasia of right posterior arch and complete aplasia of the anterior arch. C_1 left C_1 lateral mass, *Oc* occipital condyle. **b** 3-D rendering of the cervical spine from the front. Left lateral mass and left posterior arch of C_1 (*L Post Arch*) are seen, but there is no equivalent structures on the right side except for a small ossified bead-like structure (*arrow*) lateral to the lateral mass of C_2. Note intact condyle–C_1 joint on the left but free-floating occipital condyle on the right. Anterior C_1 arch is also absent. **c** Sagittal CT reconstruction showing intact articulation between left occipital condyle (*Oc*) and C_1 lateral mass (C_1). Right condyle is free floating

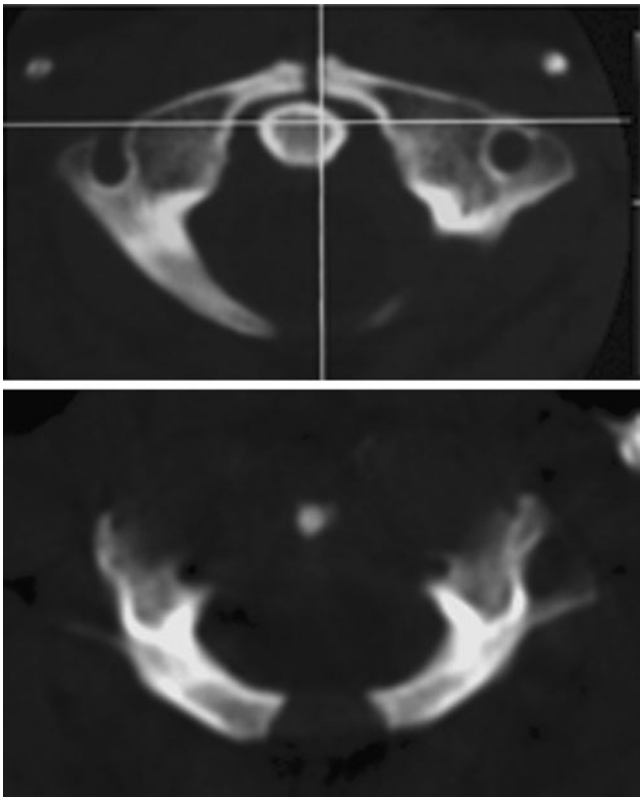

Fig. 58 Bifid anterior and posterior atlantal arches

tomatic cases is stabilization between occiput and C_2–C_3 in concert with treatment for the other associated malformations.

Unfused occipital condyle and clivus—posterior homeotic transformation

Unilateral or bilateral non-fusion of the occipital condyle with the skull base has been described [60]. The result is usually an unstable atlanto-occipital articulation and bony distortion around the joint that could indent the brainstem. Occasionally, only the clivus is unfused and the dens is fused to the anterior atlantal arch as if the atlas is acquiring its own centrum (Fig. 50). These phenotypes are reminiscent of the transgenic murine mutant with disturbance in *Hox d-4* expression and posterior homeotic transformation of the craniovertebral transitional zone, in which the exoccipital region contains unfused neural arch-like structures resembling the posterior arch of C_1, and C_1 acquires a centrum instead of an anterior arch (Fig. 22). Treatment of these rare entities consists of bony resection when necessary, followed by occipital–cervical fusion in case of instability.

Anomalies of the C_1 resegmentated sclerotome

Aplasia and hypoplasia of the C_1 hypochordal bow—anomalies of anterior atlantal arch

Aplasia of the hypochordal bow of the C_1 sclerotome leads to complete absence of the anterior atlantal arch. This is an exceedingly rare anomaly; only a few post-mortem cases can be found in the literature, in which the anterior arch was replaced by loose connective tissue [28, 49, 94]. The centrum primordium of C_1 is often simultaneously affected. Our one example of absent anterior C_1 arch is clinically unstable because the basal dental segment is unintegrated in the midline, and the two "hemi-os" are stunted. The insertion tubercles of the TAL are either greatly attenuated or non-existent, and the TAL itself may also be absent since it is derived from mesenchyme adjacent to that of the hypochordal bow and centrum. It is not visualized on MRI in our case (Fig. 51a). The result is severe anterior subluxation of C_1 on C_2 with cord compression (Fig. 51b).

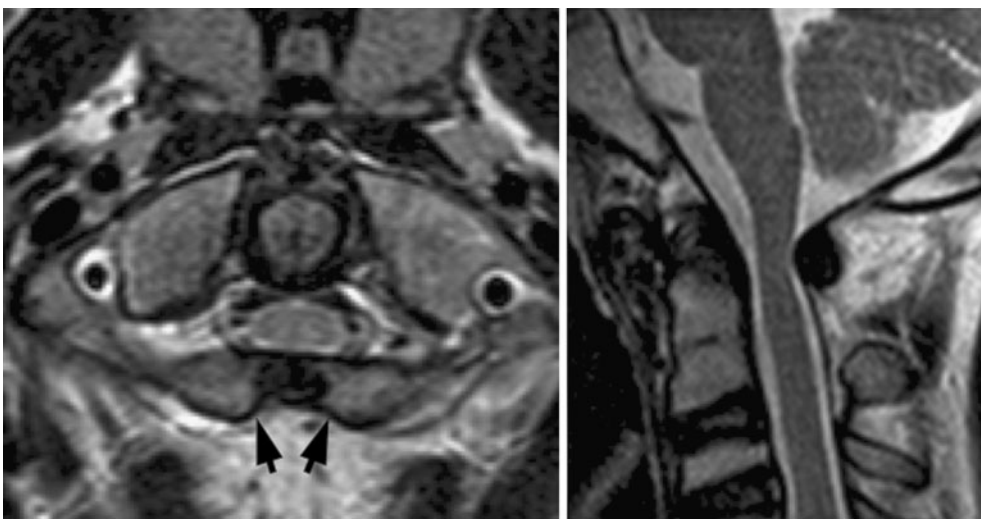

Fig. 59 Bifid posterior atlantal arch with hyperplasia and inward curling of the free ends (*arrows*) of the open arch. There is some narrowing of the spinal canal and slight indentation of the posterior surface of the cord

When blighted development of the hypochordal bow is accompanied by complete aplasia of the primordium of the C_1 centrum, the result is an extremely unstable C_1–C_2 complex. Our example shows a match-head-sized remnant of the C_1 anterior arch in front of an axial body without any dental pivot (Fig. 52). The child presented with quadriparesis.

Because the atlas in these cases is usually reduced, deformed and feeble, posterior instrument fusion needs to incorporate the occiput and often has to be extended down to C_3 or C_4 to distribute the stresses on the upright plates. If the child is very young with a large head and puny nuchal musculature, post-operative halo is recommended.

Aplasia and hypoplasia of the lateral C_1 sclerotome—anomalies of posterior atlantal arch

Varying degrees of aplasia of the lateral sclerotome of C_1 result in partial or complete agenesis of the posterior atlantal arch. Posterior atlantal arch deficiencies are ten times more common than anterior arch defects [22, 55, 56]. von Torklus and Gehle [93] documented six subtypes, the rarest being total agenesis. The example of total agenesis given here has no bony arch posterior to the lateral masses, and the anterior arch is bifid (Fig. 53). Partial agenesis can be unilateral (Fig. 54) or bilateral with preservation of all or portions of the posterior tubercle, which appears floating without bony attachment to the rest of the C_1 vertebra (Fig. 55a, b). MRI may suggest presence of cartilage in the scaffolding of the incomplete ring, but in our case, rather ample tilting of the lateral masses away from the remaining posterior tubercle during flexion (Fig. 55c) suggests that the cartilaginous mold was never formed, and the developmental error probably occurred at the mesenchymal (membranous) stage [9, 50, 81].

Unlike with aplasia of the hypochordal bow and anterior arch defects, the centrum sclerotome of C_1 is not affected in posterior arch defects. The dental pivot and TAL anchorage are thus normal (Fig. 53). The C_1–C_2 complex in patients with posterior arch defects are usually stable, in spite of the intimidating appearance of the radiographs. None of our patients require fusion.

Combined dysplasia of the hypochordal bow and lateral sclerotome of C_1-combined anterior and posterior atlantal arch defects and lateral mass aplasia

Simultaneous hypoplasia of the hypochordal bow and lateral sclerotome of C_1 leads to combined anterior and posterior atlantal defects. The anterior arcual defect is usually incomplete and the insertion tubercles and TAL are mostly intact, thereby maintaining stability against translation. However, because the two lateral masses are essentially loose bones connected by incompetent soft tissues, axial loading forces can split them apart similar to the mechanism of a Jefferson's fracture (Fig. 56).

One rare entity that is at least potentially unstable is complete aplasia of the lateral mass combined with absence of the anterior atlantal arch. The head is tilted on the side of the aplasia and usually somewhat rotated to the opposite side due to the unusual orientation of the condyle–C_2 joint (Fig. 57). This egregiously awkward articulation is unstable in limiting lateral sliding motion and rotation. Also, the inevitable loss of TAL anchorage due either to absence of the ligament or of its insertion tubercle must result in excessive translation of C_1 on C_2.

Bifid ventral and dorsal atlantal arches

Midline gaps in the dorsal atlantal tubercle are common incidental findings. Anterior bifid C_1 arch is less common but probably just as innocuous. Combined anterior and posterior C_1 bifidity is uncommon (Fig. 58). The examples we have seen are all stable entities, though the gaps never close with age. Rare cases with in-curling of the free ends of the unfused posterior arches have been known to compress the spinal cord [22] and require surgical decompression (Fig. 59).

References

1. Aoyoma H, Asamoto K (1988) Determination of somite cells: independence of cell differentiation and morphogenesis. Development 104:15–28
2. Bagnall KM (1992) The migration and distribution of somite cells after labelling with the carbocyanine dye, DiI: the relationship of this distribution to segmentation in the vertebrate body. Anat Embryol (Berl) 185:317–324
3. Bagnall KM, Sander EJ (1989) The binding pattern of peanut lectin associated with sclerotome migration and the formation of the verteral axis in the chick embryo. Anat Embryol (Berl) 180:505–513
4. Bellairs R (1980) The segmentation of somites in the chick embryo. Bolletino di zoologia 47:245–252
5. Burwood RJ (1970) The cranio-cervical junction. Anatomy. Thesis. University of Bristol
6. Cattell JS, Filtzer DL (1965) Pseudosubluxation and other normal variations in the cervical spine in children. J Bone Jt Surg Am 47A:1295–1309
7. Cave AJE (1938) The morphological constitution of the odontoid process. J Anat 72:621
8. Chevrel JP (1965) Occipitalization of the atlas. Arch Orthop Trauma Surg 13:104–108
9. Chigira M, Kaneko K, Mashio D, Watanabe H (1994) Congenital hypoplasia of the arch of the atlas with abnormal segmentation of the cervical spine. Arch Orthop Trauma Surg 113:110–112

10. Christ B, Jacob HJ, Jacob M (1978) On the formation of the myotomes in avian embryos. An experimental and scanning electron microscope study. Experentia 34:514–516
11. Christ B, Jacob HJ, Siefert R (1988) Über die Entwicklung der Zervikookzipitalen Übergangsregion. In: Hohmann D, Kügelgen B, Liebig K (eds) Neuroorthopädie. Springer, Berlin, pp 13–22
12. Christ B, Wilting J (1992) From somites to vertebral column. Ann Anat 174:23–32
13. Condie B, Capecchi MR (1993) Mice homozygous for a targeted disruption of *Hox d-3* (Hox-4.1) exhibit anterior transformations of the first and second cervical vertebrae, the atlas and axis. Development 119:579–595
14. Couly GF, Coltey PM, Le Douarin NM (1993) The triple origin of skull in higher vertebrates: a study in quail-chick chimeras. Development 117:409–429
15. Crockard H, Stevens M (1995) Craniovertebral junction anomalies in inherited disorder: part of the syndrome or caused by the disorder? Eur J Pediatr 154:504–512
16. Dalgleish AE (1985) A study of the development of thoracic vertebrae in the mouse assisted by autoradiography. Acta Anat (Basel) 122:91–98
17. David KM, Crockard A (2005) Congenital malformations of the base of the skull, atlas and dens. In: Benzel EC (ed) The cervical spine. Lippincott Williams and Wilkins, Philadelphia, pp 415–426
18. David KM, Thorogood P, Stevens JM, Crockard HA (1997) The one bone spine: a failure of notochord/sclerotome signaling? Clin Dysmorphol 6(4):303–314
19. David KM, Thorogood PV, Stevens JM, Crockard A (1999) The dysmorphic cervical spine in Klippel–Feil syndrome: interpretations from developmental biology. Neurosurg Focus 6(6):e1
20. Davis GK, Jaramillo CA, Patel NH (2001) Pax group III genes and the evolution of insect pair-rule patterning. Development 128:3445–3458
21. Davis GK, Patel NH (1999) The origin and evolution of segmentation. Trends Cell Biol 24(12):M68–72
22. Devi BI, Shenoy SN, Panigrahi MK, Chandramouli BA, Das BS, Jayakumar PN (1997) Anomaly of arch of atlas—a rare cause of symptomatic canal stenosis in children. Pediatr Neurosurg 26:214–218
23. Dietrich S, Gruss P (1995) Undulated Phenotypes suggest a role of *Pax-1* for the development of vertebral and extravertebral structures. Dev Biol 167:529–548
24. Dietrich S, Kessel M (1997) The vertebral column. In: Thorogood P (ed) Embryos, genes and birth defects. Wiley, Chichester, pp 281–302
25. Dietrich S, Schubert FR, Gruss P (1993) Altered Pax gene expression in notochord mutants of the mouse: the notochord is required for the dorsoventral patterning of the somite. Mech Dev 44:189–207
26. Dubrulle J, McGrew MJ, Pourquié O (2001) FGF signaling controls somite boundary position and regulates segmentation clock control of spatiotemporal Hox gene activation. Cell 106:219–232
27. Forsberg H, Crozet F, Brown NA (1998) Waves of mouse lunatic fringe expression, in four-hour cycles at two-hour intervals, preced somite boundary formation. Curr Biol 8:1027–1030
28. Geipel P (1955) Zur Kenntnis der Spaltbildungen des Atlas und Epistropheus. Teil IV Zbl Path 94:19
29. George AW (1919) A method for more accurate study of injuries to the atlas and axis. N Engl J Med Surg 181:395–398
30. Gholve PA, Hosalker HS, Ricchetti ET, Pollock AN, Dormans JP, Drummond DS (2007) Occipitalization of the atlas in children, morphologic classification, associations, and clinical relevance. J Bone Jt Surg Am 89:571–578
31. Giacomini C (1886) Sull' esistenza dell' "osodontoideum: nell" uomo. Gior dr Accaddi med Torino 49:24–28
32. Grabb PA, Mapstone TB, Oakes WJ (1999) Ventral brainstem compression in pediatric and young adult patients with Chiari I malformations. Neurosurgery 44:520–528
33. Haack H, Kessel M (1994) Homeobox genes and skeletal patterning. In: Hall BK (ed) Bone. CRC, Boca Raton, pp 119–144
34. Hawkins RJ, Fielding JW, Thompson WJ (1976) Os odontoideum: congenital or acquired? J Bone Jt Surg Am 38:413–414
35. Hensinger RN (1986) Osseous anomalies of the craniovertebral junction. Spine 11:323–333
36. Hensinger RN, Fielding JW, Hawkins RJ (1978) Congenital anomalies of the odontoid process. Orthop Clin North Am 9:901–912
37. Huang R, Zhi Q, Ordahl CP, Christ B (1997) The fate of the first avian somite. Anat Embryol (Berlin) 195:435–449
38. Jacob M, Christ B, Jacob HJ (1975) Über die regionale Determination des paraxialen Mesoderms junger Hühnerembryonen. Verhandlungen der Anatomischen Gesellschaft (Germany) 69:263–269
39. Jenkins JFA (1969) The evolution and development of the dens of the mammalian axis. Anat Rec 164:173–184
40. Jones FS, Georges C, Guss P, Edelman GM (1991) Activation of the cytotactin promoter by the homeobox-containing gene *Evx-1*. Proc Natl Acad Sci USA 89:2091
41. Jones FS, Prediger EA, Dennis BA, DeRobertis EM, Edelman GM (1991) Cell adhesion molecules as targets for Hox genes: neural cell adhesion molecule promoter activity is modulated by cotransfection with *Hox 2.5* and *2.4*. Proc Natl Acad Sci USA 89:2091
42. Kessel M (1992) Respecification of vertebral identities by retinoic acid. Development 115:487–501
43. Kessel M, Gruss P (1991) Homeotic transformation of murine bertebrae and concimitant alteration of *Hox* codes induced by retinoic acid. Cell 67:1–20
44. Keynes RJ, Stern CD (1988) Mechanisms of vertebrate segmentation. Development 103:413–429
45. Kieny M, Mauger A, Sengel P (1972) Early regionalization of the somitic mesoderm as studied by the development of the axial skeleton of the chick embryo. Dev Biol 28:42–161
46. Kirlew KA, Hathout GM, Reiter SD, Gold RH (1993) Os odontoideum in identical twins: perspective on etiology. Skeletal Radiol 22:525–527
47. Koseki H, Wallin J, Wilting J, Mizutani Y, Kispert A, Ebensperger C, Herrmann BG, Christ B, Balling R (1993) A role for *Pax-1* as mediator of notochordal signals during the dorsoventral specification of vertebrae. Development 119:649–660
48. Kotil D, Kalayci M (2005) Ventral cervicomedullary junction compression secondary to condylus occipitalis (median occipital condyle), a rare entity. J Spinal Disord Tech 18(4):382–385
49. Le Double AF (1903 u. 1912) Traité des variations des os du crane de l'homme et de leur signification au point de vue de l'Anthropologie zoologique. Vigot Frères, Paris
50. Logan WW, Stuard ID (1973) Absence of posterior arch of the atlas. Am J Roentgenol 118:431–434
51. Lufkin T, Mark M, Hart CP, Dollé P, LeMeur M, Chambon P (1992) Homeotic transformation of the occipital bones of the skull by ectopic expression of a homeobox gene. Nature 359:835–841
52. Macalister A (1893) Notes on the development and variations of the atlas. J Anat Physiol 27:519–542
53. Markuske H (1978) Untersuchungen zur Static und Dynamik der kindlichen Halswirbelsäule: Der Aussagewert seitlicher Röntgenaufnahmen. Die Wirbelsäule in Forschung und Praxis 50. Hippokrates, Stuttgart
54. McGrew MJ, Dale JK, Fraboulet S, Pourquié O (1998) The lunatic fringe gene is a target of the molecular clock linked

to somite segmentation in avian embryos. Curr Biol 8:979–982
55. McRae DL (1953) Bony abnormalities in the region of the foramen magnum; correlation of the anatomic and neurologic findings. Acta Radiol 40:335–354
56. McRae DL (1960) The significance of abnormalities of the cervical spine. Am J Roentgenol 84:3–25
57. McRae DL, Barnum AS (1953) Occipitalization of the atlas. Am J Roentgenol Radium Ther Nucl Med 70:23–46
58. Menezes AH (1996) Congenital and acquired abnormalities of the craniovertebral junction. In: Youmans JR (ed) Neurological surgery. WB Saunders, Philadelphia, pp 1035–1089
59. Menezes AH (1998) Embryology, development, and classification of disorders of the craniovertebral junction. In: Dickman CA, Sonntag VKH, Spetzler RF (eds) Surgery of the craniovertebral junction. Thieme, New York, pp 3–12
60. Menezes AH, Fenoy KA (2009) Remnants of occipital vertebrae: proatlas segmentation abnormalities. Neurosurgery 64:945–953
61. Menezes AH, Ryken TC (1992) Craniovertebral abnormalities in Down's syndrome. Neurosurgery 18:24–33
62. Morgan MK, Onofrio BM, Bender CE (1989) Familial os odontoideum. Case report. J Neurosurg 70:636–639
63. Müller F, O'Rahilly R (1980) The human chondrocranium at the end of the embryonic period, proper, with particular reference to the nervous system. Am J Anat 159:33–58
64. Müller F, O'Rahilly R (1994) Occipitocervical segmentation in staged human embryos. J Anat 185:251–258
65. Müller F, O'Rahilly R (2003) Segmentation in staged human embryos: the occipitocervical region revisited. J Anat 203:251–258
66. Musil L, Goodenough D (1990) Gap junctional intercellular communication and the regulation of connexin expression and function. Curr Opin Cell Biol 2:875
67. Nishikawa M, Sakamoto H, Hakuba A, Nakanishi N, Inoue Y (1997) Pathogenesis of Chiari malformation: a morphometric study of the posterior cranial fossa. J Neurosurg 86:40–47
68. Palmeirim I, Henrique D, Ish-Horowicz D, Pourquié O (1997) Avian hairy gene expression identifies a molecular clock linked to vertebrate segmentation and somitogenesis. Cell 91:639–648
69. Pendergrass EP, Schaeffer JP, Hodes PJ (1956) The head and neck in Roentgen diagnosis. Charles C. Thomas, Springfield, pp 1529–1530
70. Pollack I, Pang D, Albright LA, Krieger D (1992) Outcome following hind brain decompression of symptomatic Chiari malformations in children previously shunted with myelomeningoceles. J Neurosurg 77:881–888
71. Pollack I, Pang D, Kocoshis S, Putnam P (1992) Neurogenic dysphagia resulting from Chiari malformations. Neurosurgery 30:709–719
72. Pourquié O (2003) The segmentation clock: converting embryonic time into spatial pattern. Science 301:328–330
73. Pourquié O (2003) Vertebrate somitogenesis: a novel paradigm for animal segmentation? Int J Dev Biol 47:597–603
74. Prescher A (1990) The differential diagnosis of isolated ossicles in the region of the dens axis. Gegenbaurs Morphol Jahrb 136:139–154
75. Prescher A (1997) The craniocervical junction in man, the osseous variations, their significance and differential diagnosis. Ann Anat 179:1–19
76. Prescher A, Brors D, Adam G (1996) Anatomic and radiologic appearance of several variants of the craniocervical junction. Skull Base Surg 6:83–94
77. Rao P (2002) Median (third) occipital condyle. Clin Anat 15:148–151
78. Reiter A (1944) Die Frühentwicklung der menschlichen Wirbelsäule. II. Mitteilung: Die Entwicklung der occipitalsegmente und der Halswirbelsäule. Z Anat Entwickl 113:66–104
79. Remak R (1855) Untersuchungen über die Entwicklung der Wirbeltiere, Berlin
80. Sawada A, Shinya M, Jiang YJ, Kawakami A, Kuroiwa A, Takeda H (2001) Fgf/MAPK signaling is a crucial positional cue in somite boundary formation. Development 128:4873–4880
81. Schulze P, Buurman R (1980) Absence of the posterior arch of the atlas. Am J Roentgenol 134:178–180
82. Sensenig EC (1957) The development of the occipital and cervical segments and their associated structures in human embryos. Contrib Embryol 36:152–161
83. Smith CA, Tuan RS (1994) Human PAX gene expression and development of the vertebral column. Clin Orthop 302:241–250
84. Stapleton P, Weith A, Urbanek P, Kozmik Z, Busslinger M (1993) Chromosomal localization of seven PAX genes and cloning of a novel family member, PAX-9. Nat Genet 3:292
85. Starck D (1979) Das Skelettsystem. In: Starck D (ed) Vergleichende Anatomie der Wirbeltiere. Springer, Berlin, pp 44–95
86. Stern CD, Keynes RJ (1987) Interactions between somite cells; the formation and maintenance of segment boundaries in the chick embryo. Development 99:261–272
87. Stover LJ, Bergan U, Nilsen G, Sjaastad O (1993) Posterior cranial fossa dimensions in the Chiari I malformation: relation to pathogenesis and clinical presentation. Neuroradiology 35:113–118
88. Tramontano-Guerritore G (1927) Die atlanto-occipital union. Anat Anz 64:173–184
89. Tubbs RS, Iskandar BJ, Bartolucci AA, Oakes WJ (2004) A critical analysis of the Chiari 1.5 malformation. J Neurosurg 101:179–183
90. Vega A, Quintana F, Berciano J (1990) Basichondrocranium anomalies in adult Chiari type I malformation: a morphometric study. J Neurol Sci 99:137–145
91. von Ebner E (1888) Urwirbel und Neugliederung der Wirbelsäule. Sitzungsber Akad Wiss Wein III 97:194–206
92. von Ludinghausen M, Schindler G, Kageyama I, Pomaroli A (2002) The third occipital condyle, a constituent part of a median occipito-atlanto-odontoid joint: a case report. Surg Radiol Anat 24:71–76
93. von Torklus D, Gehle W (1969) Neue Perspektiven der Entwicklungsstörungen der oberen Halswirlbelsäule. Z Orthop 105:178
94. von Torklus D, Gehle W (1972) Anomalies and malformations. In: von Torklus D, Gehle W (eds) The upper cervical spine. Thieme, Stuttgart, pp 14–53
95. von Torklus D, Gehle W (1975) Die Obere Halswirbelsäule. Thieme, Stuttgart
96. Wadia NH (1967) Myelopathy complicating congenital atlantoaxial dislocation (a study of 28 cases). Brain 90:449–472
97. Wallin J, Mizutani Y, Imai K, Miyashita N, Moriwaki K, Taniguchi M, Koseki H, Balling R (1993) A new Pax gene, Pax-9, maps to mouse chromosome 12. Mamm Genome 4:354–358
98. Wallin J, Wilting J, Koseki H, Fritsch R, Christ B, Balling R (1994) The role of Pax-1 in axial skeleton development. Development 120:1109–1121
99. Wilting J, Ebensperger C, Müller TS, Koseki H, Wallin J, Christ B (1995) Pax-1 in the development of the cervico-occipital transitional zone. Anat Embryol (Berl) 192:221–227
100. Wollin DG (1963) The os odontoideum: separate odontoid process. J Bone Jt Surg Am Vol 45:1459–1484